

Charge Transport in Doped Conjugated Polymers for Organic Thermoelectrics

Dorothea Scheunemann^{1,2*}, Emmy Järsvall¹, Jian Liu¹, Davide Beretta³, Simone Fabiano⁴, Mario Caironi⁵, Martijn Kemerink^{2,6}, Christian Müller^{1*}

¹ Department of Chemistry and Chemical Engineering, Chalmers University of Technology, 41296 Göteborg, Sweden

² Centre for Advanced Materials, Heidelberg University, Im Neuenheimer Feld 225, 69120 Heidelberg, Germany

³ Empa, Swiss Federal Laboratories for Materials Science and Technology, Ueberlandstrasse 129, 8600 Dübendorf, Switzerland

⁴ Laboratory of Organic Electronics, Department of Science and Technology, Linköping University, Norrköping, Sweden

⁵ Center for Nano Science and Technology@PoliMi, Istituto Italiano di Tecnologia, Via Pascoli 70/3, Milano 20133, Italy

⁶ Department of Physics, Chemistry and Biology, Linköping University, Linköping, Sweden.

* dorothea.scheunemann@cam.uni-heidelberg.de; christian.muller@chalmers.se

ABSTRACT

Research on conjugated polymers for thermoelectric applications has made tremendous progress in recent years, which is accompanied by surging interest in molecular doping as a means to achieve the high electrical conductivities that are required. A detailed understanding of the complex relationship between the doping process, the structural as well as energetic properties of the polymer films, and the resulting thermoelectric behavior is slowly emerging. This review summarizes recent developments and strategies that permit enhancing the electrical conductivity of p- and n-type conjugated polymers via molecular doping. The impact of the chemical design of both the polymer and the dopant, the processing conditions, and the resulting nanostructure on the doping efficiency and stability of the doped state are discussed. Attention is paid to the interdependence of the electrical and thermal transport characteristics of semiconductor host-dopant systems as well as the Seebeck coefficient. Strategies that permit to improve the thermoelectric performance, such as uniaxial alignment of the polymer backbone, both in bulk and thin film geometries, manipulation of the dielectric constant of the polymer, and variation of the dopant size are explored. A combination

of theory and experiment is predicted to yield new chemical design principles and processing schemes that will ultimately give rise to the next generation of organic thermoelectric materials.

Keywords: molecular doping, conjugated polymer, organic thermoelectrics, Seebeck coefficient, thermal conductivity

1. Introduction

Thermoelectric materials enable direct conversion between heat and electricity by converting a temperature difference into an electrical potential via the so-called Seebeck effect.¹ The energy conversion efficiency of a thermoelectric material can be described by a dimensionless figure of merit:

$$zT = \frac{\alpha^2 \sigma T}{\kappa} \quad (1.1)$$

where α is the Seebeck coefficient, σ is the electrical conductivity, T is the absolute temperature, and κ is the thermal conductivity. Instead of zT , the power factor $\alpha^2 \sigma$ is often used to evaluate the performance of different thermoelectric materials.

Both the electrical conductivity as well as the Seebeck coefficient are related to the density of states (DOS), denoted as $g(E)$, of the system and the location of the Fermi level E_F . Following the derivation of Fritzsche,² the Seebeck coefficient of a semiconductor can be defined as the average entropy per charge carrier weighted by its contribution to the total electrical conductivity:

$$\alpha = -\frac{k_B}{q} \int dE \left(\frac{E - E_F}{k_B T} \right) \left(\frac{-\partial f}{\partial E} \right) \frac{\sigma'(E)}{\sigma} \quad (1.2)$$

where k_B is the Boltzmann constant, f is the Fermi distribution function, q is the elementary charge and $\sigma'(E)$ is the energy dependent conductivity distribution function which is related to the electrical conductivity via:

$$\sigma = \int dE \left(\frac{-\partial f}{\partial E} \right) \sigma'(E) \quad (1.3)$$

with $\sigma'(E) = q \cdot g(E) f(E) \mu(E)$ and $\mu(E)$ being the energy dependent mobility distribution. As both α and σ depend on the total carrier concentration $N = \int g(E) f(E) dE$, a common representation is to plot these two parameters against each other to circumvent the often-encountered difficulty of determining the total carrier concentration. When doing so a power law scaling with:

$$\alpha \propto \sigma^m \quad (1.4)$$

as shown in Fig. 1(a) is often observed. By collecting data for a wide range of materials, Glaudell et. al suggested that $m = -1/4$.³ Such a scaling law would imply that the power factor scales according to $\alpha^2\sigma \propto \sigma^{1/2}$ (see Fig. 1b). However, significant deviations from this behavior can be found and we discuss these relationships in detail in section 5.

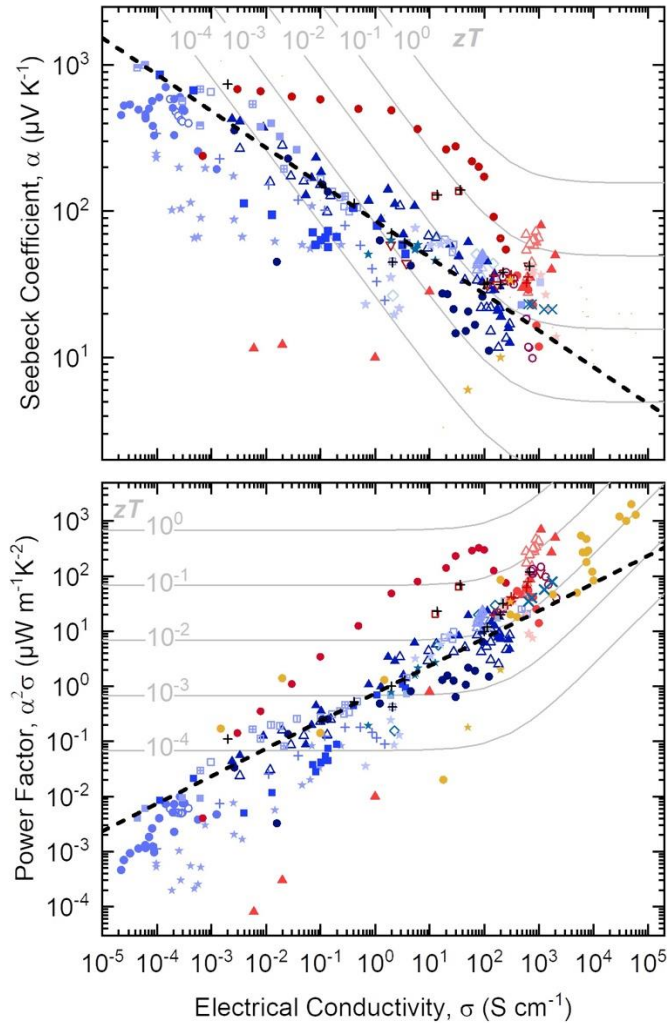


FIG. 1. Interplay of thermoelectric parameters: Seebeck coefficient α (top) and power factor $\alpha^2\sigma$ (bottom) as a function of electrical conductivity σ showing a universal trend. Data for p-type conducting polymers (blue: polythiophenes, red: poly(3,4-ethylenedioxythiophene) (PEDOT) based materials, yellow: polyacetylene) were taken from references listed in ref. 4; the dashed lines were constructed using equation 1.4 with $m = -1/4$; grey isolines corresponding to different figures of merit zT were drawn using equation 6.4 with $T = 300$ K and $\kappa_{ph} = 0.2$ W m⁻¹ K⁻¹. Reproduced with permission from Mater. Sci. Eng. R Rep. 138 (2019). Copyright 2019 Elsevier.

In consequence, many authors assume that for an organic thermoelectric material the power factor increases with its electrical conductivity,^{3,4} and hence research currently focuses on maximizing the latter. As discussed above, the electrical conductivity depends on both the mobility and the carrier concentration. However, in case of conjugated polymers the intrinsic carrier concentration is generally low. An effective way to tune the carrier concentration and conductivity of conjugated polymers over several orders of magnitude, i.e. from 10^{-5} S cm⁻¹ (e.g. oxygen-doped poly(3-hexylthiophene) (P3HT)⁵) to 10^4 - 10^5 S cm⁻¹ (polyacetylene,^{6,7} rubbed PBTTT⁸), is molecular doping.

How exactly molecular doping influences the electrical conductivity as well as other thermoelectric parameters, and thus ultimately the figure of merit, is however challenging to predict. On the one hand, several factors such as the energy landscape of the host-dopant system, its dielectric properties and the resulting nanostructure influence transport processes and the Seebeck coefficient. On the other hand, the parameters that determine zT are interdependent and optimizing one of them tends to compromise the others. As a result, there appears to be an optimal range of about $\sigma \approx 10^2$ to 10^3 S cm⁻¹ with respect to zT [cf. electronic contribution to the thermal conductivity in section 6], as can be seen from the iso- zT lines in Fig. 1b. Moreover, each of the thermoelectric parameters is temperature dependent and hence zT will also vary with temperature.

This review focuses on the impact of doping on various parameters affecting the electrical conductivity, but also the Seebeck coefficient and the thermal conductivity of conjugated polymers. The chemical structures of all polymers and dopants discussed in this review are depicted in Fig. 2.

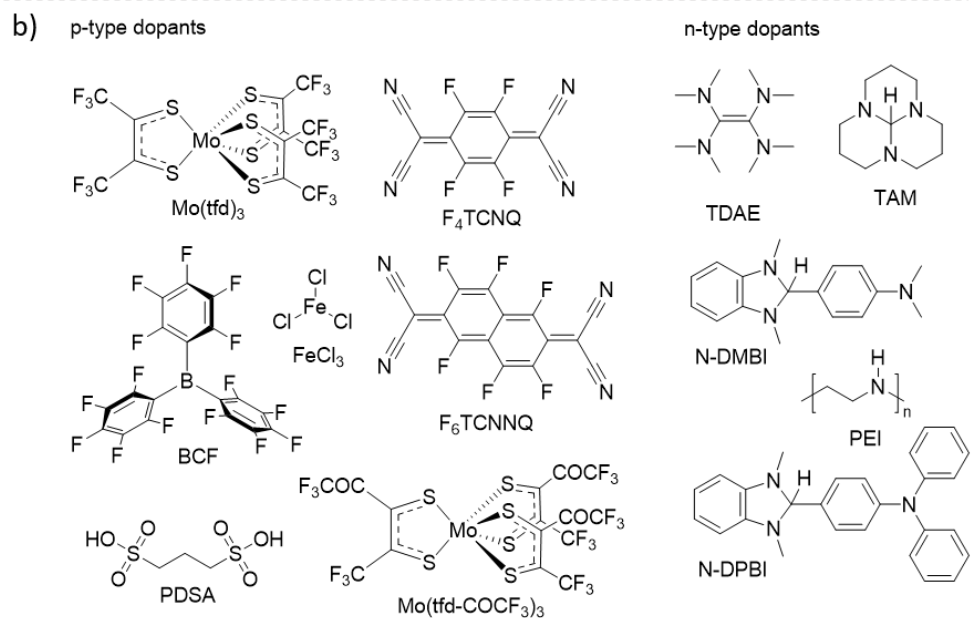
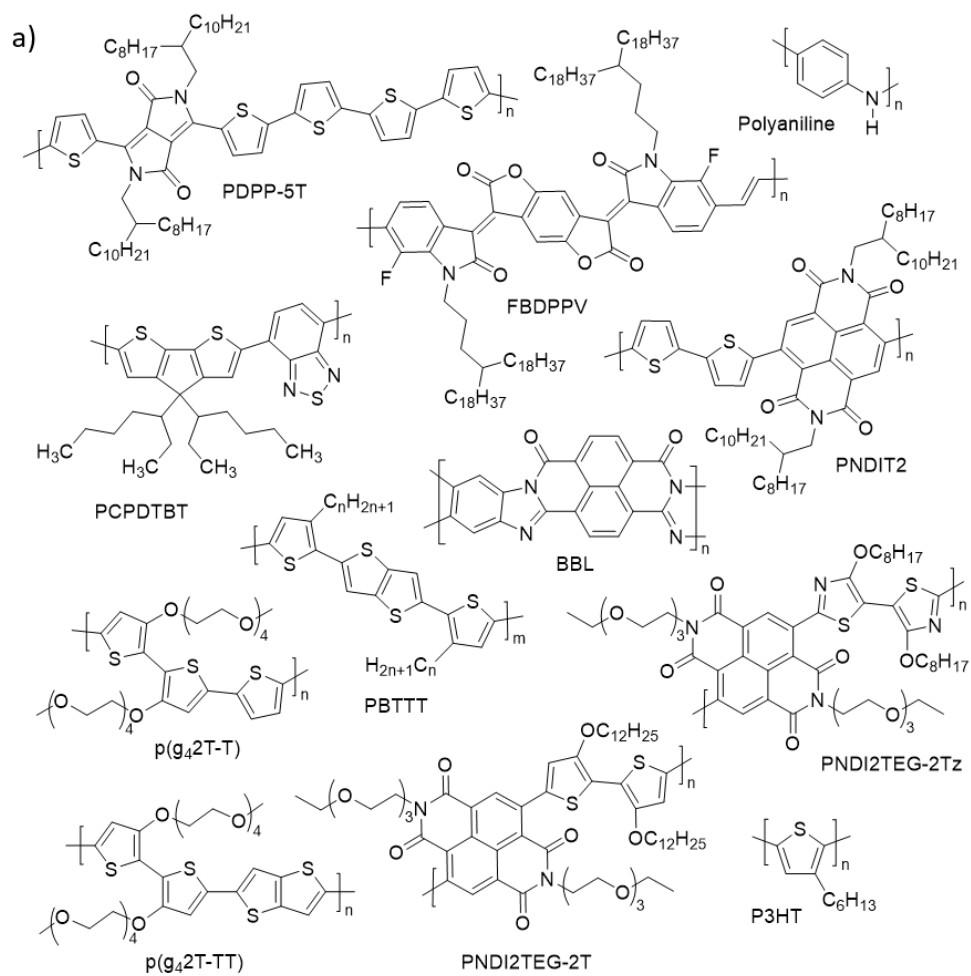


FIG. 2. Chemical structures of (a) conjugated polymers and (b) dopants discussed within this review.

We would like to point out that there are other types of materials, notably poly(3,4-ethylenedioxythiophene):poly(styrenesulfonate) (PEDOT:PSS) and poly(3,4-ethylenedioxythiophene):tosylate (PEDOT:Tos), where the conducting form of the polymer is created through oxidative polymerization,⁹ resulting in p-type conductors that can display a power factor $\alpha^2\sigma \gg 100 \mu\text{W m}^{-1} \text{K}^{-2}$ and a figure of merit $zT > 0.2$.¹⁰⁻¹² We refer the reader to recent reviews that discuss PEDOT-based materials in detail.¹³⁻¹⁵

Here, we focus on molecularly doped materials whose thermoelectric properties can be widely tuned through chemical design of both the polymer as well as the dopant molecules.

2. Molecular Doping

Molecular doping of conjugated polymers involves the addition of a chemical species that can undergo charge transfer with the host material. Many dopants can directly exchange a charge with the polymer. Redox active molecules are capable of either accepting or donating an electron from/to the polymer, which leads to p- and n-doping, respectively. Instead, the charge can also be transferred in the form of a proton (H^+) or hydride (H^-): some polymers such as polyaniline¹⁶ and polythiophenes¹⁷ can accept a proton from an acid and hence become p-doped while some semiconductors such as fullerenes¹⁸ and amide- or ester-rigidified bis(styryl)benzene derivatives¹⁹ become n-doped when they receive a hydride from DMBI-based dopants (see Fig. 2 for chemical structures).^{18, 20} A similar mechanism has been proposed for, e.g., the naphthalenediimide (NDI)-based copolymer PNDIT2 [see Fig. 2],^{18, 20} although never confirmed experimentally. It was instead argued that for weak hydride acceptors such as PNDIT2, a thermally-activated homolytic C–H bond cleavage ($\text{C–H} \rightarrow \text{C}^\cdot + \text{H}^\cdot$) has a more significant impact.²¹ Recently, the use of transition metals of the group 8-11 elements has been shown to catalyze the heterolytic cleavage of the N-DMBI-H ($\text{C–H} \rightarrow \text{C}^+ + \text{H}^-$) bond, enabling greatly increased doping efficiency.²² Other p-doping mechanisms involve a second species such as atmospheric oxygen or water that either act as the actual oxidant or first react with the dopant to form an active compound that then undergoes charge transfer with the polymer. Examples include acid mediated oxidation through oxygen²³ and doping with the Lewis acid tris(pentafluorophenyl)borane (BCF), which first forms a complex with water that then donates a proton to the polymer, followed by an additional electron transfer with an adjacent polymer chain.^{24, 25} The variety of doping mechanisms that can take place have been reviewed in detail.^{26, 27} In the remainder of this review, we will focus on direct electron transfer, which is the mechanism that is encountered when using a wide range of molecular dopants.

2.1. Degree of Charge Transfer and Ionization Efficiency

A dopant and host can undergo integer or partial electron transfer and then form an ion pair or charge-transfer complex (CTC), respectively.^{28, 29} In case of integer charge transfer the charge that is created on the polymer chain, referred to as a polaron, is balanced by the opposite charge on the dopant molecule, which now takes on the role of the counterion. The polaron and counterion form an ion pair that remains Coulombically bound. Not every dopant molecule that is introduced to the host experiences electron transfer, for example because of aggregation or variations in the energy levels of the host matrix (cf. discussion below). The ionization efficiency, which is typically less than 100%, is given by:

$$\eta_{\text{ion}} = \frac{N_{\text{polaron}}}{N_{\text{dopant}}} \quad (2.1)$$

where N_{polaron} and N_{dopant} are the number of generated polarons and dopant molecules per unit volume. While N_{dopant} is known *a priori*, especially in case of co-processing [cf. section 3.6], at low to moderate doping levels N_{polaron} can be estimated with a number of techniques such as electron paramagnetic resonance (EPR)³⁰ or optical spectroscopy.^{25, 31-33} However, caution should be paid to changes in film texture or polaron delocalization with doping level, which can for example alter the infrared absorption spectrum of polarons.^{34, 35}

Ion-pair formation is facilitated by a favorable offset between relevant energy levels of the two species. In case of p-doping the organic semiconductor donates an electron from its highest occupied molecular orbital (HOMO) to the lowest unoccupied molecular orbital (LUMO) of the (typically neutral) dopant, which readily occurs if the electron affinity of the latter (EA_{dopant}) is equal to or higher than the ionization energy of the former (IE_{osc}), i.e. $EA_{\text{dopant}} \geq IE_{\text{osc}}$ (Fig. 3(a)). For n-doping to occur, the opposite constellation is beneficial, i.e. the electron affinity of the organic semiconductor (EA_{osc}) should be equal to or larger than the ionization energy of the dopant (IE_{dopant}), i.e. $EA_{\text{osc}} \geq IE_{\text{dopant}}$ (Fig. 3(a)). The EA and IE of the dopant and host can be accurately determined with photoelectron spectroscopy or estimated using electrochemical methods such as cyclic voltammetry. However, values obtained for each individual species should only be used as an approximate guide to predict if electron transfer is energetically favorable since polarization and electrostatic interactions arise when placing the dopant in the host matrix, which can significantly alter the energy levels by up to 1 eV.³⁶ Besides, electrostatic interactions can be expected to stabilize the counterion-polaron pair²⁹ and hence may influence η_{ion} , which may be noticeable when comparing dopants with different sizes. Further, organic materials tend to show a high degree of structural and energetic disorder, which –as well as doping induced disorder– leads to a broadening of the DOS and hence allows electron transfer

despite an unfavorable offset between the nominal energy levels measured with, e.g., electrochemical methods.^{28, 37} For weak p-dopants with $EA_{\text{dopant}} < IE_{\text{osc}}$ broadening of the density of states can lead to an increase in η_{ion} with the dopant concentration.^{37, 38}

CTC formation, as schematically depicted in Fig. 3(b), involves hybridization of the frontier orbitals of the organic semiconductor and dopant and does not have any specific requirements on the energy levels of the two species. Hence, CTC formation can occur when ion-pair formation is not favored, e.g. if $EA_{\text{dopant}} < IE_{\text{osc}}$ in case of p-doping, but also when the energy offset allows the latter. For systems where CTC and ion-pair formation compete, aspects such as the nanostructure of the semiconductor^{39, 40} and the degree of overlap of the frontier orbitals of the dopant and semiconductor^{17, 41} determine which process dominates. While a CTC is neutral, it can in a subsequent step undergo electron transfer with an adjacent organic semiconductor site, and thus create a polaron, provided that its energy levels allow integer charge transfer.⁴² Since doping via CTC formation is a two-step process the ionization efficiency is typically low, i.e. $\eta_{\text{ion}} \ll 100\%$.

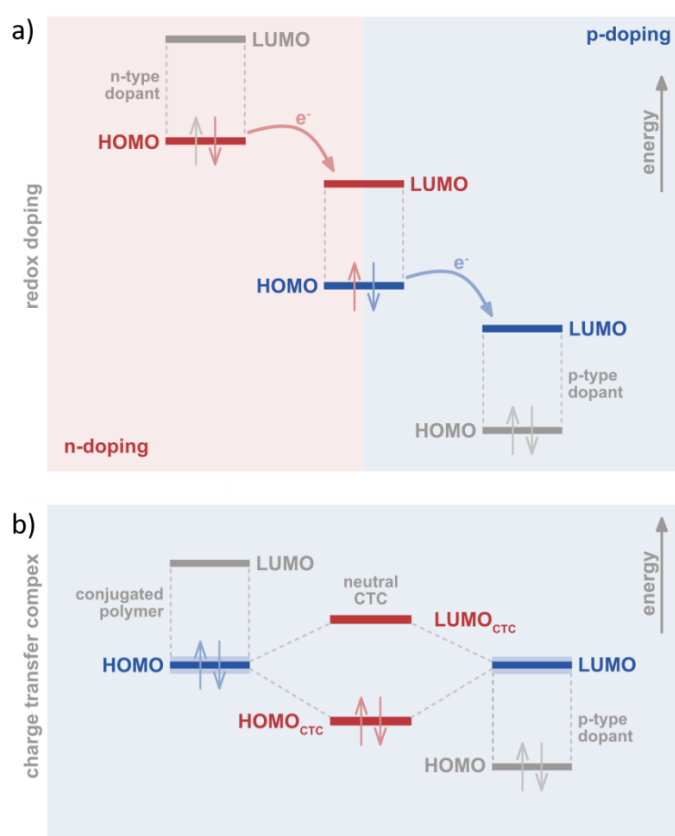


FIG. 3. Influence of frontier orbitals on molecular doping processes: (a) Basic principle of redox doping involving the transfer of an electron (e^-) from the semiconductor HOMO to the dopant

LUMO in case of p-doping and (b) the formation of a charge-transfer complex through fractional charge transfer.

While many dopants are neutral species, electron transfer with the host can also be facilitated by radical cations^{31, 43, 44} or anions⁴⁵ provided they have suitable energy levels. Accordingly, for some combinations of semiconductor and dopant, such as F₄TCNQ and polythiophenes with a sufficiently low IE, two electron transfer events can occur, where the initially neutral dopant molecule exchanges a first electron with the host followed by the exchange of a second electron between the generated counterion and a further host site.⁴⁵ This type of double doping can result in an ionization efficiency of up to 200%.

2.2. Dissociation

Polarons that form as a result of doping remain strongly bound to the counterion. These ion pairs must dissociate to generate free charges that can move in the host and contribute to charge transport. The dissociation efficiency is given by:

$$\eta_{diss} = \frac{N_{free}}{N_{polaron}} \quad (2.2)$$

where N_{free} is the number of free charge carriers, which can be measured with admittance spectroscopy on metal-insulator-semiconductor (MIS) devices or AC-Hall measurements. We note that in case of materials with hopping-dominated transport such as doped conjugated polymers, the interpretation of AC Hall measurements is not entirely straightforward as the motion of hopping carriers can partially compensate the Hall voltage, which results in an overestimation of the carrier density.⁴⁶ The dissociation efficiency is typically much less than 100% because of the strong Coulomb binding energy between dopant and polaron, i.e. not every polaron can contribute to charge transport. The Coulomb binding energy E_C is given by:

$$E_C(r) = \frac{q^2}{4\pi\epsilon_0\epsilon_r r} \quad (2.3)$$

where q is the elementary charge, ϵ_0 the permittivity of vacuum, ϵ_r the dielectric constant of the host and r the distance between the polaron and the corresponding counterion. Assuming typical values for organic semiconductors such as $\epsilon_r \approx 3$ and $r = 1$ nm, the binding energy is on the order of 500 meV, which is much larger than the thermal energy $k_B T = 25$ meV at room temperature. Although the concept of free charges is somewhat difficult in a system with strong localization and a thermal capture radius r_{th} that often is larger than the inter-dopant distance (for the given parameters, $r_{th} \approx 20$ nm, which corresponds to a relative dopant concentration of $c = 10^{-4}$), the dissociation efficiency of dopant-counterion pairs is typically argued to be low. For example, in case of P3HT doped with F₄TCNQ, which

tend to undergo integer charge transfer, Pingel and Neher have shown that at low dopant levels only 5% of the generated ion pairs dissociate into free charge carriers and hence contribute to charge transport.⁴⁷ Molecular strategies that reduce Coulombic effects by increasing ϵ_r or the polaron-counterion distance r and thus improve η_{diss} will be discussed in sections 3.3 and 3.4.

Depending on the doping level, the energetic landscape and electrostatic interactions can strongly reduce the activation energy for dissociation.^{48, 49} At very low doping levels η_{diss} is mostly governed by the Coulomb binding energy. At intermediate doping levels the energetic disorder that is introduced by neighbouring dopant molecules can strongly reduce the activation energy to as little as a few tens of meV,⁵⁰ which is comparable to $k_B T$ and hence thermal activation results in a higher η_{diss} than what would be expected by only considering E_C . Moreover, Beljonne et al. investigated the role of interactions with the local environment on the generation of free charge carriers and found that molecular quadrupole moments of host and dopant molecules reduce the energy barrier for dissociation.⁵¹ At higher doping levels, the Coulomb potentials of counterions and polarons significantly overlap and the electronic landscape flatens, which benefits charge transport [see section 3.2]. The concept of charge dissociation however becomes ambiguous at very high doping levels, where polarons are mostly trapped by the ubiquitous counterions, meaning there are nearly no free charge carriers. However, polarons can still contribute to charge transport after escaping from the Coulomb radius of one counterion until they are captured by another counterion. In that case, kinetic Monte Carlo (kMC) simulations are required to estimate the fraction of charges $f_{transport}$ that contributes to charge transport at any time to better evaluate the doping process.^{52, 53}

2.3. Doping Efficiency

The overall doping process comprises two steps, ionization and dissociation [Fig. 4], and hence the doping efficiency is given by:

$$\eta_{doping} = \eta_{ion} \times \eta_{diss} = \frac{N_{free}}{N_{dopant}} \quad (2.4)$$

Hence, η_{doping} is limited by factors that reduce η_{ion} , such as dopant aggregation and CTC formation [see section 2.1], as well as η_{diss} , such as strong Coulomb binding between polaron and counterion [see section 2.2].

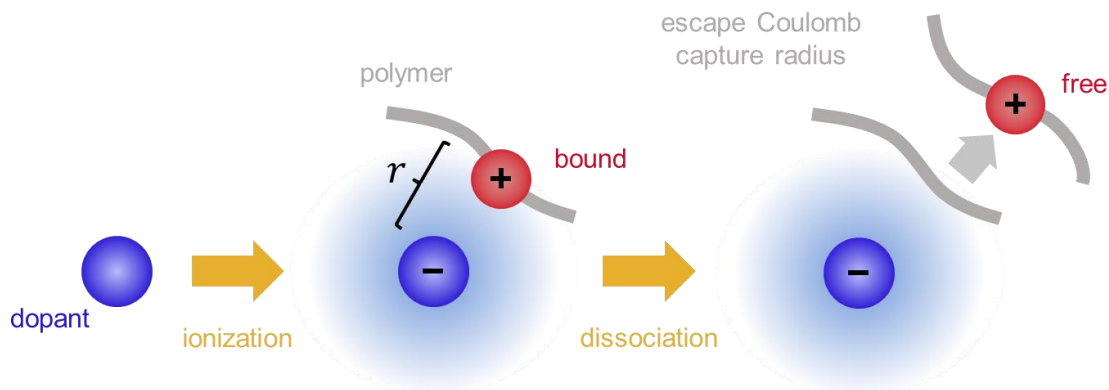


FIG. 4. Schematic illustration of the two steps of a doping process.

Since the thermoelectric performance of organic thermoelectric materials generally increases with the electrical conductivity [Fig. 1], it is important to maximize the *density* of charge carriers that contribute to transport $\rho_{transport}$, i.e. the doping level should be high. A large N_{dopant} can however lead to aggregation of dopant molecules due to limited miscibility with the host, which reduces η_{ion} and hence η_{doping} . The conducting material then consists of a fraction of dopant aggregates, which only occupy volume but do not significantly contribute to doping, which reduces $\rho_{transport}$. Synthetic strategies that allow to adjust the polarity of the polymer and/or dopant and hence improve miscibility will be discussed in section 3.5. The energy barrier for dissociation at high doping levels can be influenced by electrical screening, e.g. by selecting a material with a high ϵ_r [section 3.3], and by molecular design strategies that place the polaron and counterion further apart. It is important to keep in mind that a high $\rho_{transport}$ is needed, which means that the total volume of the conducting material constitutes an intrinsic limit. For example, a very large dopant molecule enhances η_{diss} and hence η_{doping} [cf. equation 2.4] but also occupies more space than a smaller dopant, leaving less volume that can be occupied by the charge-conducting conjugated material. Hence, there is likely an optimal dopant size for which $\rho_{transport}$ is maximized.

3. Parameters affecting charge transport and doping

3.1. Energy Offset

As discussed in section 2.1, a crucial aspect that influences doping through ion-pair formation is the energy offset ΔE between the IE and EA of the semiconductor host and dopant, i.e. $\Delta E = EA_{dopant} - IE_{osc}$ in case of p-doping and $\Delta E = EA_{osc} - IE_{dopant}$ for n-doping. For systems based on doped polymers^{54, 55} as well as small molecules³⁷ it has been observed that the ionization efficiency increases with ΔE . One challenge that is encountered when studying the effect of ΔE on the doping efficiency is the

interplay of structural and energetic effects. For instance, the size of the dopant⁵⁶ and its miscibility with the polymer matrix⁵⁷ can significantly affect η_{doping} [structural changes are discussed in sections 3.4 to 3.6]. Aubry et al. studied a molecular p-dopant system whose EA_{dopant} can be tuned over a wide range from 4.9 to 5.7 eV while maintaining the dopant size and shape, which ensures that also the Coulomb interactions between polarons and counterions remain similar.⁵⁸ An increase in the EA of the p-dopant not only resulted in an increase in ΔE but also improved the redox-driven infiltration of the p-dopant during sequential doping, which, overall, led to a higher doping level. Likewise, Jacobs et al. observed that σ increases with $\Delta E = EA_{dopant} - IE_{osc}$ for ion-exchange doping of PBTTT with a series of p-dopants with EA_{dopant} ranging from 5.2 to 5.9 eV, likely because of an increase in $N_{polaron}$ and, possibly η_{diss} , which involved sequential doping by a molecular dopant that was dissolved in acetonitrile together with an excess amount of an ionic liquid, leading to ion-exchange of the dopant counterion and the anion of the ionic liquid subsequent to the doping reaction.⁵⁹ When discussing the influence of energetics on ionization of the semiconductor, it is important to keep in mind that electrostatic interactions can strongly alter the energy levels, as discussed in section 2.1. Further, the semiconductor matrix can display a complex nanostructure, for example disordered and ordered domains in a polymer film, with a locally changing IE_{osc} and EA_{osc} . As a result, a certain dopant may only be able to undergo electron transfer with certain parts of a polymer film, e.g. the crystalline domains in polythiophenes, which have a lower IE_{osc} than disordered regions.⁶⁰

In a carefully optimized system, an η_{ion} close to 100% can be achieved at low doping concentrations via co-processing or sequential processing, meaning that each dopant ion gives rise to one polaron.^{54, 61} In case of high doping concentrations, however, many dopant molecules tend to aggregate, which leads to a reduction in η_{ion} , since now some of the dopant molecules do not undergo electron transfer with the semiconductor. The limit of $\eta_{ion} = 100\%$ can be surpassed through *double doping* if the ΔE is large, on the order of at least 0.5 eV. This is because dopants such as F₄TCNQ experience a reduction in electron affinity when they accept an electron, i.e. from $EA_{dopant} = 5.2$ eV to $EA_{anion} = 4.7$ eV. As a result, polythiophenes such as the thienothiophene-bithiophene copolymer p(g₄2T-TT) [see Fig. 2 for chemical structure], which features a low $IE_{osc} = 4.5$ eV, can donate an electron to both neutral F₄TCNQ as well as its anion since $EA_{dopant} > EA_{anion} > IE_{osc}$.⁴⁵ Double doping permits an η_{ion} of up to 200% and in case of low doping levels η_{doping} of up to 200%. Tools that allow to reach a higher doping efficiency may allow to reduce the concentration of counterions in the semiconductor and therefore minimize the perturbation of the energetic landscape of the host [see section 3.5].

3.2. Density of States and Disorder

In intrinsic, undoped materials the density of states (DOS) is assumed to be (either exponential or) Gaussian in shape:

$$g_i(E) = \frac{N_0}{\sqrt{2\pi\sigma_{DOS}^2}} \exp\left(\frac{-(E_i - E_0)^2}{2\sigma_{DOS}^2}\right) \quad (3.1)$$

where E_i is the single particle energy of site i , σ_{DOS} the energetic disorder of the Gaussian DOS, and N_0 is the total site density. Upon doping the shape of the DOS however changes as a consequence of the long range of the Coulomb potential of ionized dopants and the low dielectric constants of most organic semiconductors. An approximation for such an ion-perturbed DOS of a doped semiconductor at low to moderate doping levels, where Coulomb traps can be considered as independent, was developed by Arkhipov et al.,^{62, 63} as:

$$g(E) = A \int_{-\infty}^0 \frac{dE_C}{E_C^4} \exp\left(\frac{A}{3E_C^3}\right) g_i(E - E_C), \quad (3.2)$$

where $A = 4\pi q^6 N_{\text{dopant}} / (4\pi\epsilon_0\epsilon_r)^3$. Pingel and Neher used the resulting mobility model to fit the dependence of the electrical conductivity on the doping ratio of P3HT:F₄TCNQ films.⁴⁷

Zuo et al. extended equation 3.2 to account for energy level differences between the dopant and the semiconductor, i.e. $\Delta E = EA_{\text{dopant}} - E_i$ in case of p-doping and $\Delta E = E_i - IE_{\text{dopant}}$.^{5, 64}

$$\begin{aligned} g(E) &= \left(1 - \frac{4\pi N_d}{3N_i}\right) \frac{g_1(E)}{\int_{-\infty}^0 dE g_1(E)} + \frac{4\pi N_d}{3N_i} \frac{g_2(E)}{\int_{-\infty}^0 dE g_2(E)} \quad (3.3) \\ g_1(E) &= A \int_{E_1}^0 \frac{dE_C}{E_C^4} \exp\left(\frac{A}{3E_C^3}\right) g_i(E - E_C) \\ g_2(E) &= A \int_{-\infty}^{E_1} \frac{dE_C}{E_C^4} \exp\left(\frac{A}{3E_C^3}\right) g_i(E - \Delta E - E_C), \end{aligned}$$

where $E_1 = E_C (N_i^{-1/3})$ is the Coulomb energy one lattice constant away from the ionized dopant. The purpose of this extension is to construct a DOS, which contains weighted parts that reflect both the host material (g_1) and the dopant (g_2). It is worth noting that both Eq. (3.2) and (3.3) do neither consider contributions of non-nearest dopant ions to the Coulomb energy nor long-range Coulomb interactions between mobile charges. However, Zuo et al. demonstrated that the model presented in equation (3.3) shows, up to a relative dopant concentration of 10^{-2} , good agreement with numerically accurate kMC simulations that include both effects. At high doping levels, however, these Coulomb

interactions as well as the effect of double occupation on the DOS have to be taken into account in order to correctly describe the experimentally measured DOS.^{65, 66} In addition, it was recently shown that, assuming an energy-dependent localization length, a semi-analytical model based on a Gaussian disorder model can qualitatively describe experimentally observed power-law trends of $\sigma(N)$ even at medium to high doping concentrations. The energy dependence of the localization length was determined on the basis of numerically exact solutions of a tight binding model.⁶⁷

Fig. 5(a) shows a Gaussian DOS broadened by Coulombic interactions as described by equation 3.3. Such a broadening of the DOS upon doping has been confirmed experimentally using photoelectron spectroscopy.⁶⁸⁻⁷⁰

As argued in section 2, polarons have to overcome the Coulomb energy barrier in order to contribute to charge transport. Several studies showed that electrostatic energetic disorder induced by neighboring counterions can facilitate this escape process.^{5, 49, 50} At sufficiently high doping levels, the Coulomb potentials of individual counterions overlap [see Fig. 5(b)], which flattens the energy landscape and promotes the escape of carriers from long-range traps. Using kMC simulations Fedai et al. demonstrated that the intrinsic and doping-induced disorder correlate. Hence, the modification of the DOS is governed by disorder compensation effects.⁷¹ For highly disordered materials the additional disorder introduced by doping can overcompensate the intrinsic disorder of the material. As a result, the total disorder remains constant or is even reduced.

An additional effect of doping induced disorder is that even nominally weak dopants can be almost fully ionized. In this context it was shown by kinetic Monte Carlo simulations that the ionization of weak dopants can be a disorder-activated process in organic materials, while it is temperature activated in inorganic semiconductors.³⁸ In turn this implies that the energy offset between the frontier orbitals of the dopant and host are less important than commonly assumed (section 3.1).

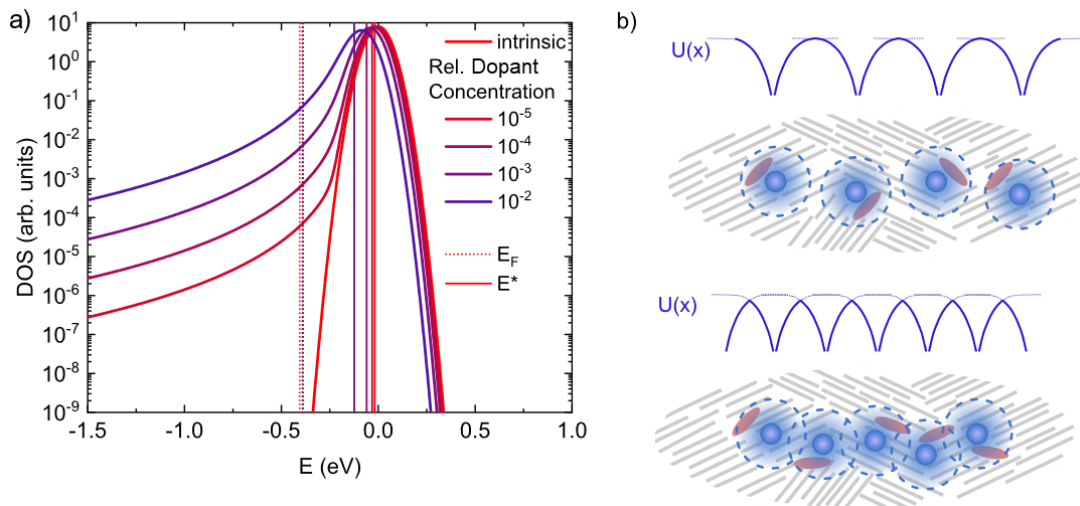


FIG. 5. Impact of doping on the density of states (DOS): Effect of low to moderate doping on a Gaussian DOS (energetic disorder $\sigma_{\text{DOS}} = 50$ meV) of a disordered organic semiconductor (a) and effect of a high doping level on the Coulomb potential overlap (b). Thin dashed and solid lines in (a) indicate the Fermi Energy E_f and the transport energy E^* , respectively. (b) (top) Negligible overlap of the Coulomb potentials $U(x)$ of counterions at a low doping level leads to large barriers ϕ for detrapping (bottom) while significant overlap at a sufficiently high doping level flattens the energy landscape.

3.3. Impact of the Dielectric Constant on Charge Transport

At high doping levels, which are needed for the design of thermoelectric materials, the charge on the polymer, i.e. the polaron, cannot move sufficiently far away from the dopant counterion to escape its Coulomb radius, without feeling the influence of another counterion [section 2.2]. Hence, the continuous interaction of polarons and surrounding dopant counterions (as well as other charges) must be considered. As a result, charge transport is dominated by the collective interactions between all charges within the conducting material. The extent to which a charge feels the presence of counterions in its vicinity depends, to a first approximation, on the dielectric constant of the *medium*. According to equation 2.3, an increase in dielectric constant will reduce the Coulomb binding energy that is felt by the polaron in the vicinity of a polaron, i.e. partial electrical screening results in a less strongly bound polaron. It can therefore be anticipated that the dielectric constant influences charge transport in doped conjugated polymers.

The dielectric constant of conjugated polymers can be adjusted through a variety of means. Strategies that are currently under investigation include partial fluorination of the polymer

backbone,⁷²⁻⁷⁵ modification of non-polar alkyl side chains with polar sulfinyl, sulfonyl or cyano groups,^{73, 76-78} and the replacement of non-polar side chains with more polar oligoether side chains.⁷⁹⁻⁸³ Functional groups associated with strong local permanent dipoles may itself constitute a Coulomb trap. Cyano groups positioned at the end of alkyl side chains, for instance, increase the energetic disorder, which reduces the hole mobility deduced from space-charge limited current (SCLC) measurements by about two orders of magnitude.⁷³ The use of oligoether side chains appears to be a better choice for increasing the overall dielectric permittivity that is felt by a polaron traversing a doped polymeric material, since local variations in electric field are likely to be less pronounced. An additional advantage of oligoether side chains, as discussed in section 3.5, is the improved compatibility of polar polymers with dopant molecules.

A comparison of polythiophenes with alkyl or oligoether side chains, doped with the same molecular dopant, indicates that the latter tend to display a higher electrical conductivity. For example, doping of p(g₄2T-T)⁸⁴ with F₄TCNQ yields an electrical conductivity of up to 100 S cm⁻¹,⁸⁵ which is two to typically ten-fold higher than values reported for F₄TCNQ doped P3HT.⁸⁶⁻⁹⁰ The polar tetraethylene glycol side chains of p(g₄2T-T) bestow the polymer with a higher $\epsilon_r = 4.4$ as compared to P3HT with $\epsilon_r = 2.7$.⁹¹ The higher dielectric constant in case of p(g₄2T-T) can be expected to enhance screening of dopant anions such as F₄TCNQ (di)anions, which are thought to be located between the side chains of the polymer.^{86, 91-95} As a result, it is feasible that polarons on the polythiophene backbone are less strongly influenced by the counterions surrounding the polymer, which would result in a higher charge-carrier mobility and hence electrical conductivity (cf. equation 1.3).

To support this argument, we vapor-doped thin films of P3HT and p(g₄2T-T) using a reported procedure⁸⁸ and determined the variable-temperature electrical conductivity $\sigma(T)$, which we fitted with a previously described analytical variable range hopping (VRH).^{5, 64, 96} The good agreement of the experimental data and the VRH model, which takes the difference in ϵ_r and oxidation level into account [Table 1 and Fig. 6], is consistent with the projected positive influence of a higher ϵ_r on $\sigma(T)$. The size of ϵ_r has an influence on the DOS as described in section 3.2. An increase of the dielectric permittivity decreases the Coulomb interactions and thus leads to a smaller width of the DOS. We anticipate that in-depth studies, which elucidate the impact of the local dielectric environment on charge transport, rather than treating the material as a dielectric continuum, will provide invaluable insights with regard to, e.g., the optimal choice of side chains. In this context, we would like to highlight the recent theoretical work by Comin et al., which shows that high doping levels lead to a strong increase in dielectric constant and large fluctuations at the microscopic scale.⁹⁷

Table 1. Parameters obtained from fitting the variable-temperature conductivity $\sigma(T)$ of F₄TCNQ vapor doped P3HT and p(g₄2T-T) shown in Fig. 6, with the VRH model described in refs. ^{5, 64, 96}, using fixed values of the dielectric constant ϵ_r from ref. ⁹¹, and treating the attempt-to-hop frequency ν_0 , localization length of the wavefunction α^{-1} , mean inter-site distance on a cubic lattice a_{NN} and dopant-induced carrier density N as free parameters. Here $N = c/a_{NN}^3$ with c the relative dopant concentration assuming that each dopant produces one charge.

	P3HT	p(g ₄ 2T-T)
ϵ_r	2.7	4.4
Gaussian disorder (meV)	78	55
ν_0 (10^{13} s^{-1})	2.7	9.5
α^{-1} (nm)	0.93	0.42
a_{NN} (nm)	2.8	1.3
N (10^{26} m^{-3})	0.2	0.6

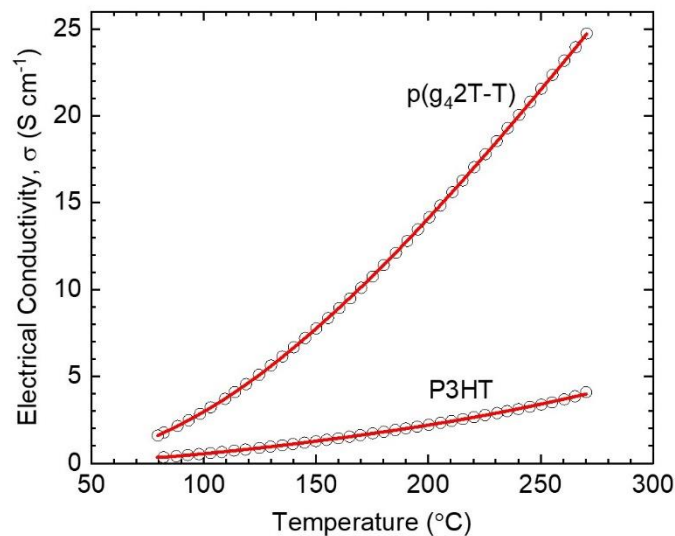


FIG. 6. Impact of the dielectric constant on the electrical conductivity: Variable-temperature electrical conductivity σ (open symbols), and analytical fit using the VRH model described in refs. ^{5, 64, 96} with the fit parameters given in Table 1, and using experimentally determined values for ϵ_r of P3HT (regioregularity $\approx 96\%$, $M_n \approx 29 \text{ kg mol}^{-1}$; PDI ≈ 2.2 ; 70 nm thin film spin-coated from 1:1 chlorobenzene:*o*-dichlorobenzene at 60 °C) and p(g₄2T-T) ($M_n \approx 16 \text{ kg mol}^{-1}$; 85 nm thin film spin-coated from 1:1 chloroform:acetonitrile at 20 °C) vapor doped with F₄TCNQ, as described in ref. ⁸⁸.

3.4. Size of the Dopant

The size of a dopant can significantly affect the spatial separation between polarons located on the polymer backbone and the counterion, and thus the strength of the Coulomb interaction between the two species [Fig. 7(a)]. The distance between the F₄TCNQ anion and a polaron on a P3HT backbone is thought to be about 5-9 Å,³⁵ which leads to a large energy barrier for dissociation and hence a low η_{diss} . Instead, large dopants such as dodecaborane (DDB) clusters with a diameter of 20 Å, which enforces a much larger distance between the polaron and counterion, result in highly mobile carriers.⁵⁴ DDB dopants of the form B₁₂(OCH₃R)₁₂ with R being a functionalized aryl group have an EA_{dopant} that ranges from 4.9 to 5.7 eV, which yields p-dopants of different oxidation strengths.⁵⁸ DDB dopants enter crystalline domains of P3HT despite their size and yield highly mobile polarons, with η_{ion} reaching 100 % for DDB-F₇₂ with the highest EA_{dopant}.⁵⁸ The consequence of highly mobile polarons is a conductivity that is significantly improved for a given polaron density compared to material doped with a smaller reference dopant such as F₄TCNQ. The importance to physically separate counterion and polaron was also supported by kMC simulations, which show that polaron-counterion interactions lower the overall conductivity compared to the hypothetical case where no counterions are present.⁹⁶ On the other hand, large dopant molecules can induce structural changes in the polymer because they are nevertheless able to intercalate between the side chains in crystalline polymer domains.^{54, 56} Further, at high dopant concentrations aggregates of dopant molecules tend to disrupt the nanostructure of the polymer, which usually deteriorates the (thermo)electric properties [see section 3.6]. Hence, it is important to distinguish between the influence of the dopant size on polaron-counterion interactions, and the concomitant impact on the nanostructure of the semiconductor. Thomas et al. have studied vapor-doping of PBTTT with NOPF₆ followed by exchange of the anion via a sequential solution-based process, which allowed to vary the counterion size from 5.2 to 8.2 Å without significantly changing the nanostructure of the polymer.⁹⁹ While the counterion size influenced polaron delocalization, the electrical conductivity was not affected by an increase in size, which indicates that the influence of other factors such as structural order and grain boundaries on charge transport are important to consider, as recently confirmed by Jacobs et al.¹⁰⁰

Large dopants occupy more volume, which ultimately limits the polaron density [section 2.3]. The total DOS of a polymer is on the order of 10²⁷ m⁻³, i.e. the material can, at best, sustain one charge per cubic nanometer. P3HT, for example, has a density of 1.1 g cm⁻³ and therefore features 4 thiophene rings per nm⁻³. Each thiophene is, in principle, a redox site and if we assume a highest oxidation level of 33%, which is common for PEDOT,¹⁰¹ then we obtain a charge-carrier density of about 10²⁷ m⁻³. If each charge is accompanied by a dopant that is, e.g., 1 nm in diameter then the highest obtainable

charge-carrier density is about $5 \times 10^{26} \text{ m}^{-3}$, which has been reported for, e.g., P3HT doped with the molybdenum dithiolene complex $\text{Mo}(\text{tfd-COCF}_3)_3$,¹⁰² which has a size of 11 to 14 Å.

Several studies have shown that incorporating small dopants such as FeCl_3 or F_4TCNQ into P3HT can lead to a decrease in the π -stacking distance.^{34, 88, 90, 103} The origin of this reduction in the distance between adjacent polymer backbones upon doping is still under discussion. Some authors suggest geometrical arguments such as the intercalation of small molecules like F_4TCNQ between the alkyl side chains of P3HT.^{86, 92-95} However, it was also reported that upon introduction of structurally similar small molecules, which do not dope the polymer, no change in the π -stacking distance occurs.^{104, 105} This would imply that the doping process itself alters the crystalline packing motif. Liu et al. used density functional theory (DFT) to investigate this question and suggested that the delocalization of the polaron across multiple adjacent P3HT backbones leads to attractive forces that reduce the π -stacking distance.¹⁰⁶

The size of dopant molecules also influences the ability to diffuse in the polymer. On the one hand, rapid diffusion is desirable for sequential doping of polymer films with dopant solutions or dopant vapor. However, with regard to long-term stability, diffusion of dopants is not desired because it will lead to gradual changes in dopant distribution. Neutral F_4TCNQ has a diffusion coefficient D of about $10^{-11} \text{ cm}^2 \text{ s}^{-1}$ in P3HT at 40 °C, which however decreases once the dopant has accepted an electron due to the electrostatic interaction between polarons and anions, i.e. the F_4TCNQ anion features a much lower $D \approx 10^{-13} \text{ cm}^2 \text{ s}^{-1}$.¹⁰⁷ Hence, it is possible to sequentially dope polymer films, while the doped material becomes more stable due to a reduction in the diffusion coefficient [cf. section 5]. Diffusion of F_4TCNQ type dopants can be reduced further by replacing one of the cyano groups with, e.g., a methyl ester group,¹⁰⁷ which Moulé et al. have used to develop a highly sophisticated patterning technique.¹⁰⁸ F_6TCNNQ anions, which are larger than F_4TCNQ anions, display a smaller diffusion coefficient,¹⁰⁹ which can be beneficial for the stability of the doped state [see section 4].

Mixing small and large dopants might provide a way to exploit the advantages of dopants with various sizes, i.e. the ability of small dopants to diffuse more easily and the higher polaron-counterion distance facilitated by larger dopants. In this context, Liang et al. have shown that under certain conditions doping a P3HT film with a mixture of $\text{Mo}(\text{tfd})_3$ and FeCl_3 can lead to a higher power factor than doping with either of the dopants alone.⁵⁶

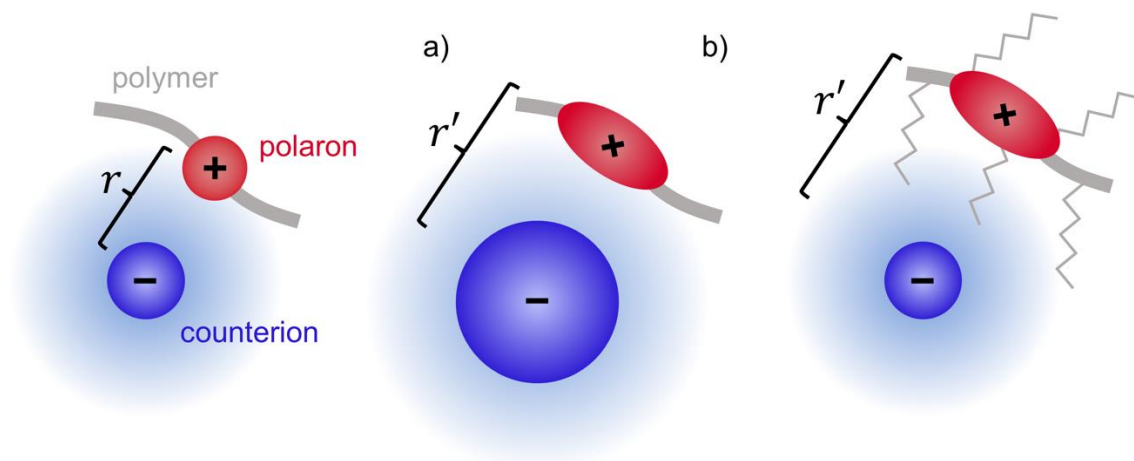


FIG. 7. (a) An increase in the size of the counterion or (b) suitable polymer side chains will increase the effective distance between a counterion and an adjacent polaron from r to r' , resulting in a less strongly bound polaron due to a lower Coulomb interaction. As a result, the polaron will delocalize to a greater extent along the conjugated polymer backbone.

3.5. Spatial Distribution of Dopant Molecules

Charge transport strongly depends on the spatial distribution of the dopant. Clustering of dopants in the polymer can lead to a heavily-tailed DOS and hence a dramatic increase in the energetic disorder, which deteriorates the electrical conductivity.¹¹⁰ Moreover, phase segregation between the polymer and the dopant can strongly limit η_{ion} [see section 2.1]. One effective strategy that allows to control the miscibility of the two species and manipulate crystallization is the choice of suitable polymer side chains. Many dopants are polar molecules and hence conjugated polymers that feature more polar oligoether instead of alkyl side chains can increase the polymer-dopant miscibility.¹¹¹ Kroon et al. attached tetraethylene glycol side chains to a polythiophene backbone [cf. structure of p(g₄2T-T) in Fig. 2], which yields a conductivity of up to 100 S cm⁻¹ when doped with F₄TCNQ¹¹¹⁻¹¹³ or different acids.²³ Oligoether side chains increase the local dielectric constant, stabilize the dopant counterions and, as a result, significantly enhance the thermal stability [cf. section 4]. However, the use of polar side chains is not a universal solution to improve the thermal stability of the doped material. In addition, the IE_{osc} of the polymer (in case of p-doping) as well as the precise interactions between dopant and the side chains must be taken into account.¹¹⁴ Many molecular dopants prefer to intercalate between the side chains and hence a reduction in the side-chain grafting density increases the space available for the counterion and hence affects η_{ion} ^{115, 116} and the thermal stability.¹¹⁷ The side-chain length is another parameter that influences polymer-dopant interactions as observed in case of PBTTT with different alkyl side chains ranging from *n*-octyl to *n*-octyldecyl.¹¹⁸

The spatial separation of the polymer backbone and dopant counterion strongly influences the extent of polaron delocalization since a more distant counterion results in a lower Coulomb binding energy [Fig. 7(b)].¹¹⁹ Spano and co-workers have studied the infrared absorption spectra of P3HT doped with F₄TCNQ and correlated the oscillator strength and peak position of polaronic absorption bands with the extent of intra- and interchain polaron delocalization, which are influenced by factors such as the molecular weight and nanostructure of the polymer.³⁵ Again, the side chains can be used to modify the distance between the counterion and backbone [see section 3.4 for effect of dopant size]. For instance, Liu et al. studied DMBI-doped NDI-based copolymers with amphiphatic side chains consisting of an alkyl spacer and an oligoether segment, which allowed to spatially separate counterions and the polymer backbone resulting in reduced Coulomb interactions.¹¹⁹ In case of donor-acceptor copolymers, charge transfer only occurs if the dopant is located next to the right moiety, e.g. next to the donor moiety in case of p-doping, as shown by Di Nuzzo et al. for PCPDTBT doped with F₄TCNQ.¹²⁰

3.6. Influence of Doping on the Nanostructure

Doping can strongly alter the nanostructure of a conjugated polymer in terms of the crystal structure, the degree of crystalline order, the crystal size and the connectivity between domains. The crystal structure of the semiconductor can change upon doping as exemplified by P3HT and PBTTT doped with F₄TCNQ, where the dopant intercalates between the side chains of the polymer.⁸⁹ Further, doping can enhance the degree of π -stacking of less ordered polymers such as p(g₄2T-T)²³ and regio-random P3HT.^{105, 121} Likewise, doping of regio-regular P3HT can change the conjugation length of polymer chains in the amorphous regions, in particular of those that make up the rigid amorphous fraction, and hence improve connectivity and the overall conductivity.¹²²

There are two principal doping methods: (1) co-processing of the polymer and dopant from the same solution and (2) sequential processing which involves casting of a polymer film followed by a doping step where the solidified film is brought in contact with a dopant solution or vapor [Fig. 8]. Co-processing allows to control the exact ratio between polymer and dopant. However, dissolving polymer and dopant in the same solvent can be challenging and the premature ionization of polymers in solution can reduce their solubility, leading to the formation of aggregates⁸⁶ that are characterized by less tie chains and hence a poor connectivity between crystalline domains, resulting in a lower charge-carrier mobility.⁸⁶ Hence, the processing solvent strongly influences the solid-state nanostructure of films obtained by, e.g., spin- or blade-coating. For instance, co-processing of P3HT with F₄TCNQ from chloroform results in a much larger degree of π -stacking and, hence η_{doping} as compared to films co-processed from chlorobenzene in case of which pre-aggregation in solution was observed.⁹⁵

Sequential processing requires that the dopant diffuses into the already solidified polymer.^{123, 124} Hence, thin polymer films can be doped rapidly, while thicker structures must be exposed to a dopant solution or vapor for long periods of time since the diffusion coefficient of many dopants in the semiconductor host is relatively low [see section 3.4]. For instance, 50 nm thin films of P3HT can be sequentially doped with Mo(tfd-COCF₃)₃ within minutes,¹⁰² while doping of tens of micrometers thick structures takes two days.¹²⁵ The two-step process ensures that the processing conditions that are used for preparation of the polymer film determine its texture and degree of in-plane orientation, which are largely preserved during the sequential doping step. For instance, P3HT films maintain an edge-on texture upon sequential processing, which benefits in-plane charge transport, while co-processing results in a more isotropic texture.^{34, 86, 94} Further, thin films that feature long-range oriented domains^{90, 126} or a high degree of in-plane uniaxial alignment^{8, 102, 109} maintain their microstructure upon doping. Similar observations have been made for bulk materials such as foams of P3HT that keep their microstructure upon sequential doping with F₄TCNQ.¹²⁷ Sequential processing can be used to elucidate structure-property relationships relevant for charge transport in doped polymers. For instance, sequential doping of P3HT thin films with F₄TCNQ has shown that the crystallinity of the polymer strongly influences the charge-carrier mobility while η_{ion} remains unaffected, overall resulting in an increase in σ but not α with the degree of order.⁸⁷ Sequential processing tends to result in a higher thermoelectric power factor than co-processing,^{90, 126} since the most optimal nanostructure can be selected prior to doping.

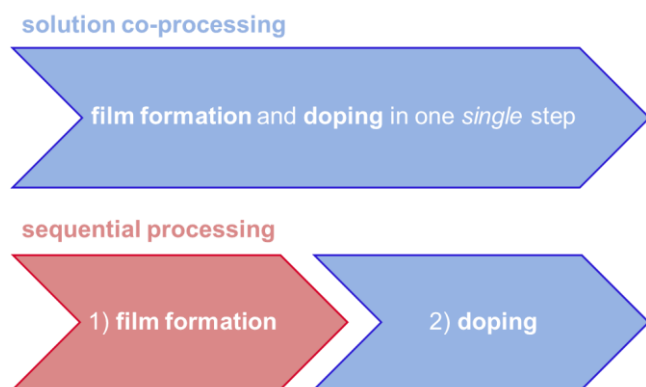


FIG. 8. Solution co-processing involves deposition of the organic semiconductor and molecular dopant from the same solution (top) while sequential processing is a two-step process where the conjugated polymer is first cast from solution followed by doping through contact with a molecular dopant dissolved in an orthogonal solvent or dopant vapor (bottom).

4. Stability of the Doped State

Thermoelectric energy harvesting requires prolonged exposure of p- and n-type materials to heat gradients, which necessitates a high degree of thermal stability. Many conjugated polymers display good chemical stability at ambient conditions but gradually undergo thermo-oxidative degradation at elevated temperatures above 100 °C, and certainly above 200 °C, unless stabilizers such as those commonly used for polyolefins are added.¹²⁸ Doped polymers with good thermal stability even at 100 °C are more difficult to realize. Hence, we argue that polymer based thermoelectric devices can only be used in combination with relatively cold heat sources whose temperature T_{hot} is less than 200 °C, which ultimately limits the generated power since $P_{out} \propto \Delta T^2 = (T_{hot} - T_{cold})^2$.^{129, 130}

The thermal stability strongly depends on the polymer:dopant pair. Some dopants are relatively small molecules with a high vapor pressure that can diffuse within a polymer,^{107, 131} which can be exploited for sequential processing [cf. section 3.6], but also implies that dopants can escape the conducting material again [Fig. 9]. F₄TCNQ, for instance, can sublime above 100 °C, which means that a F₄TCNQ-doped polymer tends to gradually return to its neat, undoped state when heated.^{40, 85} The polarity of the side chain can however improve the ability of the polymer to retain the dopant upon heating.^{85, 132} Other dopants such as 1,3-propanedisulfonic acid (PDSA) have a lower vapor pressure and therefore p(g₄2T-T) p-doped with PDSA retains its high σ of up to 120 S cm⁻¹ for at least 20 hours at 120 °C and exposure to air.²³

Some dopants undergo side reactions with the polymer. F₄TCNQ can abstract a hydrogen from P3HT—but not p(g₄2T-T)—resulting in the formation of a weak dopant, HF₄TCNQ⁻, which strongly reduces the conductivity especially upon annealing at temperatures above 100 °C.¹³³ Further, F₄TCNQ initially undergoes integer charge transfer (ICT) with polymers such as P3HT and PBTTT but gradually reverts to a thermodynamically stable CTC between the polymer and the dopant.¹³⁴ The concomitant decrease in the number of charge carriers that can contribute to transport results in a gradual decrease in conductivity. The substrate temperature during vapor-doping of PBTTT with F₄TCNQ allows to adjust the degree of CTC formation.⁴⁰ Samples with a moderate amount of CTC states retain a higher conductivity upon prolonged annealing at 100 °C because the dopant is retained by the polymer to a greater extent, resulting in a higher thermal stability of the doped state.⁴⁰

While many p-doped polymers are stable at ambient conditions, the electrical conductivity of many n-doped polymers rapidly diminishes upon exposure to air and water. Improved air stability is observed for polymers with an $EA_{osc} > 3.9$ eV. While the electrical conductivity of PNDIT2 ($EA_{osc} = 3.8$ eV) doped with N-DPBI decreases rapidly upon air exposure, a similar polymer with a lower $EA_{osc} = 4.0$ eV, achieved by thionation of the naphthalene diimide segments, shows a steady $\sigma \approx 10^{-3}$ S cm⁻¹ for at

least 1000 min at ambient conditions.¹³⁵ Thermally stable n-type materials have been reported for poly-(benzimidazobenzophenanthroline) (BBL; $E_{A_{osc}} = 4.2$ eV).⁹¹ BBL, sequentially n-doped with TDAE or N-DMBI, initially features a relatively high $\sigma \approx 2$ S cm⁻¹, which rapidly drops in case of TDAE due to the low vapor pressure of the dopant while N-DMBI doped BBL displays a stable electrical conductivity at 190 °C for at least 20 hours under nitrogen.¹³⁶ Yang et al. have recently screened a series of triaminomethane based dopants in-silico and identified one candidate, TAM [Fig. 2(b)] that was subsequently synthesized, which yielded a stable $\sigma \approx 21$ S cm⁻¹ at ambient conditions, as well as $\alpha^2\sigma \approx 51$ μ W m⁻¹ K⁻², when used to n-dope the polymer FBDPPV [see Fig. 2 for chemical structure].¹³⁷

Good thermal stability at 200 °C under nitrogen is also observed for all-polymer blends of BBL and p(g₄2T-T), which undergo ground-state electron transfer,⁹¹ or BBL and poly(ethyleneimine) (PEI),¹³⁸ resulting in conducting materials that do not contain any small-molecular dopant, which could diffuse or sublime [Fig. 9]. All-polymer blends of BBL and PEI display an electron conductivity of up to $\sigma \approx 8$ S cm⁻¹, with micrometer-thick films also showing remarkable air-stability. Overall, these polymer blends can be considered an n-type equivalent to the most widely studied p-type conducting polymer material, PEDOT:PSS.

The poor air stability of some n-doped polymers can be mitigated through encapsulation. For instance, benzodifurandione based copolymers doped with N-DMBI show a stable electrical conductivity of up to 90 S cm⁻¹ once a 500 nm thick layer of an amorphous fluoropolymer is applied that effectively protects the n-doped polymer from air.¹³⁹ A protection layer may also allow to address the high vapor pressure of some dopants by keeping dopant molecules inside the material.

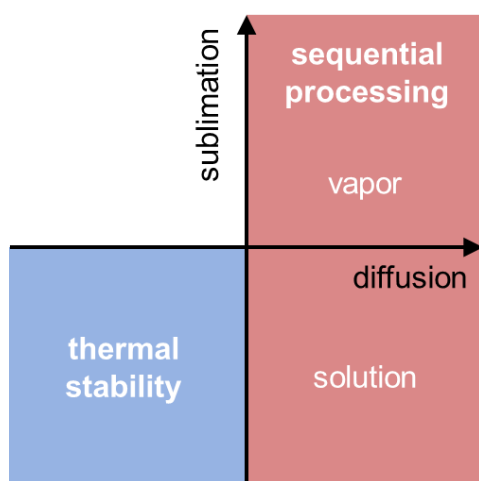


FIG. 9. Small-molecular dopants that easily sublime and display a high diffusion coefficient in the semiconductor are excellent for sequential processing (red) while larger (polymeric) dopants and/or those that strongly interact with the semiconductor may facilitate a higher degree of thermal stability (blue).

5. Effect of Doping on the Relationship Between Seebeck Coefficient and Electrical Conductivity

As discussed in the introduction, an important quantity to determine the figure of merit zT of a thermoelectric material is the power factor and thus the functional relationship between α and σ . While the general trends are well established, the details are less clear and significant deviations from the $\alpha \propto \sigma^{-1/4}$ proportionality proposed by Glauddell et al. have been reported, especially at higher doping levels. Following the discussion in section 3.2, this could at least partly arise due to dopant-induced changes to the DOS.^{110, 140} Doping can also alter the nano- and microstructure of the semiconductor [cf. sections 3.5 and 3.6]. In this context, Thomas et al. have studied electrochemical oxidation of PBTTT and found that the exponent of the α vs. σ relation can deviate from $m = -1/4$ [see section 1] even though the nanostructure was not altered.¹⁴¹ Instead, the authors argue that doping induced energetic disorder results in a broadening of the local DOS. An alternative strategy to modify the DOS distribution is blending of two semiconductors A and B with different energy levels.^{142, 143} This leads to a binary mixture A:B, exhibiting a double-peaked DOS. For an optimized mixture, the DOS can be tuned in a way that the transport energy E_{tr} is shifted into the B-part of the DOS, while the Fermi energy remains in the A-part. This leads to high thermopowers at reasonable conductivities and moreover a power factor of the mixture that can exceed that of the neat compounds.¹⁴³

It is also possible to manipulate the α vs. σ relation and with this the power factor of doped polymers using sequential processing methods that introduce uniaxial alignment in polymer films, e.g. through high-temperature rubbing or drawing, followed by doping. While several studies have shown that the resulting alignment of the polymer backbone leads to a considerable increase of the electrical conductivity along the direction of orientation [see section 3], the influence on the thermopower is less clear. Sarabia-Riquelme et. al investigated the thermoelectric properties of wet-spun PEDOT:PSS fibers and found an increase in electrical conductivity by drawing the fibers in a DMSO bath.¹⁴⁴ This increase in conductivity was attributed to a synergistic effect of a larger degree of π -stacking of PEDOT upon removal of PSS through treatment with DMSO as well as the alignment of PEDOT upon drawing. Meanwhile, α was unaffected along the direction of orientation. Similar observations were also made by other authors for PEDOT:PSS based films and fibers.^{145, 146} In contrast, several recent reports on PBTTT based thin films indicate that both α and σ can be enhanced simultaneously,^{8, 109, 118} resulting in a drastic improvement of the power factor by several orders of magnitude along the direction of orientation [Fig. 10].⁸ The α vs. σ relation has a universal shape for values measured both parallel and

perpendicular to the alignment direction that, for PBTTT, is independent of the type of dopant (F_4TCNQ , F_6TCNNQ or $FeCl_3$).¹⁰⁹ However, the side-chain length influences the degree of anisotropy in thermoelectric parameters that can be obtained.¹⁴⁷ For films of P3HT doped with F_4TCNQ it was recently shown that the degree of anisotropy in σ and α depends on the initial structure of the film and shows a discontinuity with the transition from a smectic-like to a semicrystalline phase.¹⁴⁸ In this context, it seems reasonable to expect that the experimental conditions used to align P3HT determine whether an anisotropy in α is observed^{8, 89, 102} or not.¹²⁵ The assumption that the value of α depends on the packing motif of the polymer is supported by kMC simulations,¹⁴⁷ which indicate that different lattice structures affect the degree of anisotropy in σ and α , emphasizing the importance of the nanostructure on the thermoelectric properties.

Several recent studies have observed that for both initially n- as well as p-doped polymers a sign change in the Seebeck coefficient occurs at high dopant concentrations. Hwang et al. experienced a sign change in the Seebeck coefficient in poly(pyridinium phenylene).¹⁴⁹ The authors argued that, as a result of extensive doping, the original LUMO level is fully filled and thus acts as a new HOMO level. However, this requires high dopant concentrations. In contrast, it was shown that both NDI¹⁴⁰ and DPP¹⁵⁰ based polymers, which are n-doped at low dopant concentrations, already show such a change in the Seebeck coefficient at much lower dopant concentrations. In case of the polymer PNDI2TEG-2T this behavior was explained by the formation of new mobile states upon doping that lie below the LUMO of the undoped material. Simulations suggested that the transport energy can cross the Fermi energy even at moderate dopant densities, leading to a sign change in α as long as the formed CTC states show a higher localization length than the host states, i.e. the CTC states are more delocalized.¹⁴⁰ Interestingly, in case of both polymers, PNDI2TEG-2T and PNDI2TEG-2Tz, the sign change in α disappeared upon modification of the donor moiety, which thus provides a means to tailor the DOS.¹⁴⁰

Likewise, the Seebeck coefficient of several p-doped polymers shows a sign change from positive to negative upon an increase in concentration of the oxidizing agents $FeCl_3$ or $NOBF_4$.^{65, 151} For non-oriented PDPP-5T thin films the doping concentration above which a change in the sign of α occurs increases with molecular weight. The authors attributed the sign change to state filling in a purely Gaussian DOS and modification of the width of the latter with molecular weight.¹⁵¹ However, the effect of Coulomb interactions on the shape of the DOS [see section 3.2] is ignored and, moreover, the assumed DOS is not in agreement with the ones measured in refs. ¹⁴⁰ and 65.

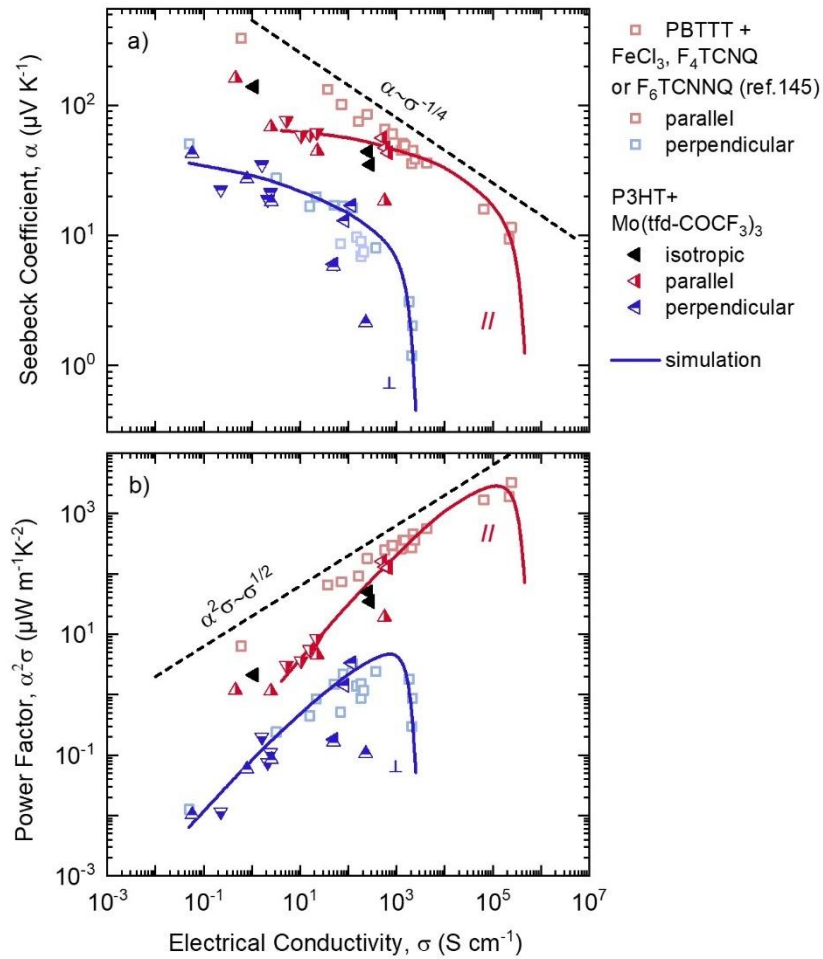


FIG. 10. Impact of uniaxial orientation on the thermoelectric parameters: (a) Seebeck coefficient α and (b) power factor $\alpha^2 \sigma$ as a function of electrical conductivity σ for P3HT (triangles) and PBTTC (squares) measured parallel (red) and perpendicular to the alignment direction (blue); black data points are values for isotropic P3HT samples. Full lines correspond to simulations based on a kMC model applied to a regular lattice, with an anisotropy ratio of $\xi_{\parallel}/\xi_{\perp} = 4$, where ξ_{\parallel} and ξ_{\perp} are the localization length parallel and perpendicular to the alignment direction, respectively (for details see ref. ¹⁴⁷). Experimental values are taken from ref. ¹⁴⁷ (\square), ref. ¹⁰² (\blacktriangleleft), ref. ⁸⁹ (\blacktriangledown) and ref. ⁸ (\blacktriangle). Note that this picture is a modified version of Figure 4 in ref. ¹⁴⁷ (D. Scheunemann, V. Vijayakumar, H. Zeng, P. Durand, N. Leclerc, M. Brinkmann, M. Kemerink, Adv. Electron. Mater., 6, 2000218, 2020; licensed under a Creative Commons Attribution (CC BY 4.0) license.), including additional data for P3HT.

6. Interplay Between Electrical and Thermal Conductivity

The thermal conductivity κ is given by the sum of the electronic contribution κ_{el} and the phonon contribution κ_{ph} .¹⁵²

$$\kappa = \kappa_{el} + \kappa_{ph} \quad (6.1)$$

Since free electrons carry both heat and charge, both σ and κ depend on the charge-carrier concentration and are hence related. The Wiedemann-Franz (WF) law,¹⁵³ which is valid for many metals and metal alloys where electrons only experience elastic scattering, states that the ratio κ_{el}/σ is approximately constant:

$$\frac{\kappa_{el}}{\sigma} = L_0 T \quad (6.2)$$

where $L_0 = \left(\frac{\pi^2}{3}\right) \left(\frac{k_B}{e}\right)^2 = 2.44 \times 10^{-8} \text{ W } \Omega \text{ K}^{-2}$ is the Sommerfeld value of the Lorenz number. Attempts to apply the WF law to disordered organic materials has met with mixed results¹⁵⁴⁻¹⁵⁶ since electronic charge transport is often dominated by inelastic hopping between redox sites. For instance, Weathers et al. have observed for suspended films of PEDOT:PSS and PEDOT:Tos that the increase of the in-plane component of κ with σ exceeds the trend predicted by the WF law for metals, which indicates significant electronic thermal transport.¹⁵⁵

To examine the ratio κ_{el}/σ in organic systems, starting from the (generalized) Miller and Abrahams hopping transfer rate,¹⁵⁷ different theories have recently been proposed, leading to the definition of new Lorenz numbers.

Assuming a system of identical molecular charge transfer sites, Craven et al. have derived a new Molecular-Wiedemann-Franz (MWF) law for amorphous molecular solids.¹⁵⁸ The MWF law states that:

$$\frac{\kappa_{el}}{\sigma} = L_M T_M \quad (6.3)$$

where $L_M = (k_B/e)^2$ is the molecular Lorenz number, and $T_M = \lambda/k_B$ is an effective temperature parameterized by the reorganization energy λ of the redox charge transfer. While the WF law is material-independent, the new MWF law implicitly depends on the temperature through λ . Since λ often depends only weakly on temperature, the MWF will be temperature-independent in most cases.

Scheunemann et al.¹⁵⁹ have extended the transport models for α and σ developed by Schmechel et al.¹⁶⁰ and Ihnatsenka et al.¹⁶¹ to κ_{el} . The extended model shows that the energetic disorder strongly influences the ratio κ_{el}/σ . In particular, κ_{el}/σ is found to be smaller than the Sommerfeld value in weakly disordered systems with high charge-carrier concentrations [see Fig. 11].

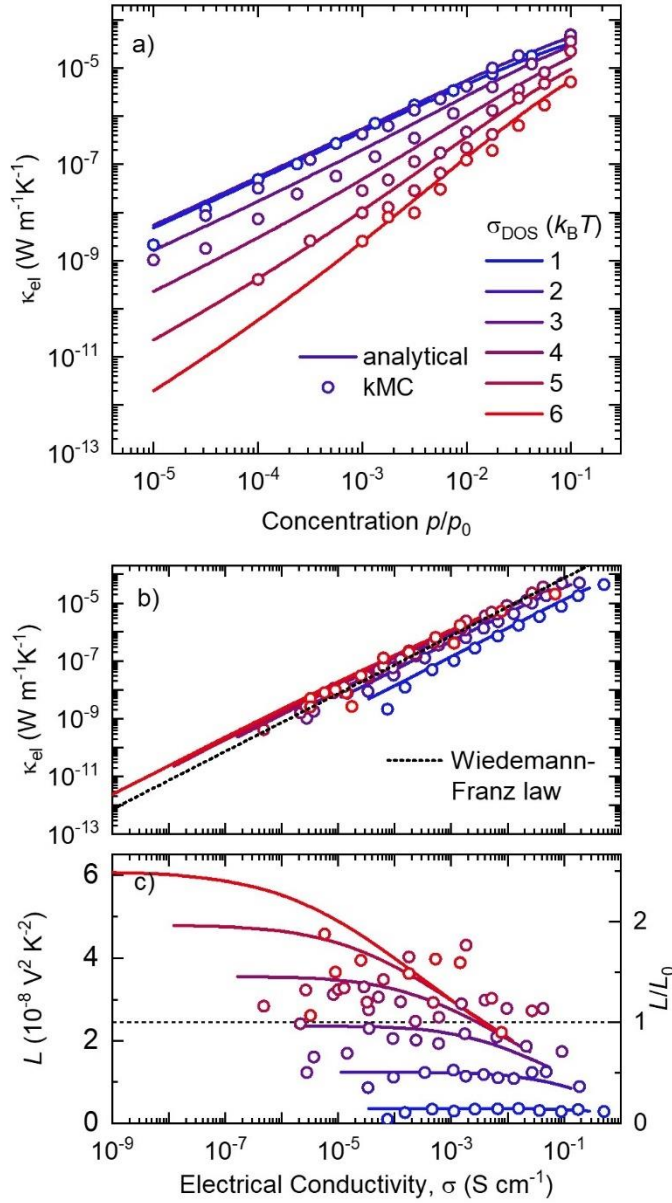


FIG. 11. Influence of doping on the thermal conductivity: κ_{el} from the analytical model (solid lines) and kMC simulations (symbols) for different energetic disorder σ_{DOS} with dependency on (a) relative carrier concentration p/p_0 and (b) electrical conductivity. The dotted black line in (b) represents the result of the WF law with $L = L_0$. (c) Lorenz number L as a function of σ . The dashed line indicates the Sommerfeld value for a free electron gas.¹⁵⁹ Figure reproduced from ref. ¹⁵⁹ (D. Scheunemann, M. Kemerink, Phys. Rev. B, 101, 075206, 2020; licensed under a Creative Commons Attribution (CC BY 4.0) license.).

The validity of the WF law in thermoelectric materials is of great interest as the ratio κ_{el}/σ naturally appears in the figure of merit zT . In fact, combining equations 1.1, 6.1 and 6.2 yields:

$$zT = \frac{\alpha^2 \sigma T}{\kappa_{ph} + \sigma \mathcal{L} \tau} \quad (6.4)$$

where \mathcal{L} is either L_0 or a non-Sommerfeld Lorenz number, which potentially is a function of the charge-carrier concentration and of the energetic disorder,¹⁵⁹ and τ is the absolute temperature T or an effective temperature T_M , depending on the model that better describes the ratio κ_{el}/σ . On the one hand, if $\kappa_{ph} \gg \sigma \mathcal{L} \tau$, then $zT \propto \alpha^2 \sigma$ and one can enhance zT by finding an optimal charge-carrier concentration that maximizes the power factor $\alpha^2 \sigma$, assuming that doping does not affect κ_{ph} . The latter may not apply in the case of molecular doping, which can alter the nanostructure and hence affect charge transport [section 3.6]. Interestingly, for PBTTT doped with F₄TCNQ, Zapata-Arteaga et al. have shown that phonon scattering through the presence of dopant molecules can reduce κ from about 0.7 to 0.4 W m⁻¹ K⁻¹.¹⁶² On the other hand, if $\kappa_{ph} \ll \sigma \mathcal{L} \tau$, then $zT \sim \alpha^2 / \mathcal{L}$ and one can enhance zT by maximizing the ratio α^2 / \mathcal{L} . The crucial parameter here is likely the Seebeck coefficient, since the square of α probably varies more than the Lorentz factor in most cases. In ref.¹⁵⁹, however, it was shown that in both cases the energetic disorder of the material is decisive for high zT values.

Recent studies show that κ_{el} becomes the dominant quantity of κ only at sufficiently high σ ,^{159,162} and that κ_{ph} should be reduced below 0.2 W m⁻¹ K⁻¹ while maintaining a large α in order to achieve a high zT .¹²⁹ In this context, Liu et al. have recently demonstrated that some fullerene derivatives, which are generally known to display a very low $\kappa_{ph} < 0.1$,¹⁶³ can maintain a high α of about -250 μ V K⁻¹ upon doping with N-DMBI, resulting in a figure of merit of up to $zT = 0.34$ at 120 °C.¹⁶⁴

Fig. 12 shows iso- zT lines at 300 K calculated according to the original WF law, to the model from Scheunemann et al., and to the model of Craven et al. (for two different values of λ). The figure shows that, depending on the model, zT benefits differently from increasing σ , and that the iso- zT lines calculated with the model of Craven et al. tend to overlap with the iso- zT lines obtained from the model of Scheunemann et al. for $\lambda \approx 0.05$ eV.

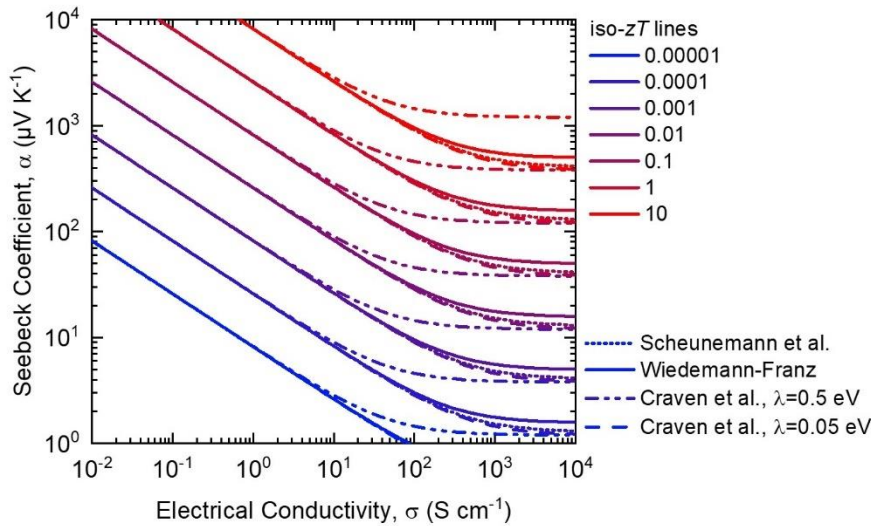


FIG. 12. Interplay of thermoelectric parameters for different models for κ_{el} : Iso- zT lines in the $\sigma - \alpha$ plane calculated according to the original WF law (continuous lines), the model of Craven et al. assuming $\lambda = 0.5 \text{ eV}$ and $\lambda = 0.05 \text{ eV}$ (dashed and dot-dashed lines, respectively), and the model from ref. ¹⁵⁹ (dotted lines) assuming $k_{ph} = 0.2 \text{ W m}^{-1} \text{ K}^{-1}$.

Organic materials can display anisotropic charge transport that depends on the nano- and microstructure [section 3.6]. Both measurements^{154, 165} and kMC simulations¹⁴⁷ have demonstrated that such a structural anisotropy can also lead to anisotropic κ_{el} . Assessment of the validity of the WF law for such anisotropic systems is not trivial as the measurement of κ and σ must be done along the same direction. The development of experimental techniques that permit to measure κ and σ along the same direction or, preferably, along all non-equivalent directions is therefore a prerequisite for gaining detailed knowledge about the relation between σ and κ_{el} . Moreover, structural anisotropy can be accompanied by significant differences in κ_{ph} in the parallel and perpendicular direction of orientation, which is reasonable when considering that changes in the nanostructure can yield a high κ_{ph} of above $1 \text{ W m}^{-1} \text{ K}^{-1}$ also for conjugated polymers.¹⁶⁶

7. Outlook

We have discussed the interplay of the semiconductor nanostructure, processing, doping efficiency and charge transport, which is increasingly well understood in qualitative terms. More work is needed to enable a complete quantitative description of the electrical properties of doped organic semiconductors, and here the dialogue between experimentalists and theorists will continue to be instrumental. For example, the impact of alignment of the semiconductor in thin-film or bulk

geometries is emerging as a powerful means that allows to not only maximize the electrical conductivity but also to constrain the complexity of doped materials, which facilitates new theoretical understanding. Rationales that aid the selection of dopants for a given organic semiconductor, and vice versa, with the aim to optimize the processability, doping efficiency and stability are slowly emerging. It can be anticipated that further synthetic work, carried out in vitro and increasingly in silico, will unearth new design principles.

A compromise will likely need to be struck with regard to the dopant size. Sufficiently small dopant molecules facilitate processing concepts such as vapor doping and enable sequential processing (doping) of thicker structures, since small molecules tend to diffuse more rapidly. On the other hand, larger molecules diffuse slowly, or not at all, which benefits the long-term stability of the doped state. In this context, the use of all-polymer systems, comprising both conjugated polymers doped or complexed with polymeric dopants or polyelectrolytes (cf. PEDOT:PSS and BBL:PEI) as well as pairs of conjugated polymers that undergo ground-state electron transfer may facilitate a new generation of stable organic conductors. All-polymeric materials may allow to circumvent the high reactivity of many redox dopants and acids, which raises both environmental concerns and prevents their use for applications in bioelectronics and wearable electronics, where benign materials are often a prerequisite.

Another aspect that we expect to grow in importance is the maximum number of charges that can be generated per given volume of material, which is limited not only by the doping efficiency but also the size of dopant molecules. Larger dopants tend to benefit charge dissociation but, on the other hand, take up a larger volume that cannot be occupied by the ionized semiconductor where charge transport ultimately occurs.

With respect to thermoelectric applications, both experimental observations and theoretical predictions have shown that fertile new avenues such as alignment of the polymer backbone and raising of the dielectric constant of a polymer benefit both the thermopower and electrical conductivity. One important question, however, is whether the resulting increase in the power factor will be accompanied by changes in the thermal conductivity. For instance, alignment of the polymer backbone can be expected to significantly increase the lattice component of the thermal conductivity. The design of new high-performance thermoelectric materials must therefore pay more attention to the still poorly understood thermal conductivity of doped polymers. In this respect, the field should continue to harness the highly productive synergies that arise through the combination of experiments and computational approaches.

Finally, we would like to point out that little attention is currently being paid to the environmental burden involved in processing from organic solvents as well as recycling of doped organic materials – and organic (semi)conductors in general– at the end of their lifetime. A complete life cycle assessment will be needed to ensure that organic thermoelectrics evolves into a sustainable technology. We argue that it would be advantageous if all types of materials that are needed to fabricate a wide range of organic electronic devices, from p- and n-type semiconductors and conductors to electrolytes and insulators, can be realized with only a handful of different materials that can, ideally, be separated again into their individual components. Ultimately, this vision may allow to develop green organic electronics that help to significantly reduce electronic waste.

Data Availability

The data that support the findings of this study are available from the corresponding author upon reasonable request.

Acknowledgements

We gratefully acknowledge financial support from the Swedish Research Council (grants no. 2016-06146 and 2018-03824), the European Union’s Horizon 2020 research and innovation programme under the Marie Skłodowska-Curie grant agreement No. 799477 (HyThermEI) and No. 955837 (HORATES) and the Knut and Alice Wallenberg Foundation through a Wallenberg Academy Fellowship Prolongation grant. We thank Jonna Hynynen for experimental contributions and Renee Kroon for synthesizing p(g₄2T-T).

References

- ¹T. J. Seebeck, “Ueber die magnetische Polarisation der Metalle und Erze durch Temperaturdifferenz,” *Annalen der Physik* **82**, 253-286 (1826).
- ²H. Fritzsche, “A general expression for the thermoelectric power,” *Solid State Commun.* **9**, 1813-1815 (1971).
- ³A. M. Glauzell, J. E. Cochran, S. N. Patel, and M. L. Chabiny, “Impact of the doping method on conductivity and thermopower in semiconducting polythiophenes,” *Adv. Energy Mater.* **5**, 1401072 (2015).
- ⁴D. Beretta, N. Neophytou, J. M. Hodges, M. G. Kanatzidis, D. Narducci, M. Martin- Gonzalez, M. Beekman, B. Balke, G. Cerretti, W. Tremel, A. Zevalkink, A. I. Hofmann, C. Müller, B. Döring, M.

- Campoy-Quiles, and M. Caironi, "Thermoelectrics: From history, a window to the future," *Mater. Sci. Eng. R Rep.* **138**, 100501 (2019).
- ⁵G. Zuo, H. Abdalla, and M. Kemerink, "Impact of doping on the density of states and the mobility in organic semiconductors," *Phys. Rev. B* **93**, 235203 (2016).
- ⁶A. J. Heeger, "Semiconducting and metallic polymers: The fourth generation of polymeric materials," *J. Phys. Chem. B* **105**, 8475-8491 (2001).
- ⁷K. Akagi, H. Shirakawa, K. Araya, A. Mukoh, and T. Narahara, "Highly conducting polyacetylene films prepared in a liquid crystal solvent," *Polym. J* **19**, 185-189 (1987).
- ⁸V. Vijayakumar, Y. Zhong, V. Untilova, M. Bahri, L. Herrmann, L. Biniek, N. Leclerc, and M. Brinkmann, "Bringing conducting polymers to high order: Toward conductivities beyond 10^5 S cm⁻¹ and thermoelectric power factors of 2 mW m⁻¹ K⁻²," *Adv. Energy Mater.* **9**, 1900266 (2019).
- ⁹A. Elschner, S. Kirchmeyer, W. Lovenich, U. Merker, and K. Reuter, *PEDOT: Principles and applications of an intrinsically conductive polymer*, CRC Press, 2010.
- ¹⁰O. Bubnova, Z. U. Khan, A. Malti, S. Braun, M. Fahlman, M. Berggren, and X. Crispin, "Optimization of the thermoelectric figure of merit in the conducting polymer poly(3,4-ethylenedioxythiophene)," *Nat. Mater* **10**, 429-433 (2011).
- ¹¹G. H. Kim, L. Shao, K. Zhang, and K. P. Pipe, "Engineered doping of organic semiconductors for enhanced thermoelectric efficiency," *Nat. Mater* **12**, 719-723 (2013).
- ¹²D. A. Mengistie, C.-H. Chen, K. M. Boopathi, F. W. Pranoto, L.-J. Li, and C.-W. Chu, "Enhanced thermoelectric performance of PEDOT:PSS flexible bulky papers by treatment with secondary dopants," *ACS Applied Materials & Interfaces* **7**, 94-100 (2015).
- ¹³O. Bubnova, and X. Crispin, "Towards polymer-based organic thermoelectric generators," *Energy Environ. Sci.* **5**, 9345-9362 (2012).
- ¹⁴Z. Fan, and J. Ouyang, "Thermoelectric properties of PEDOT:PSS," *Adv. Electron. Mater.* **5**, 1800769 (2019).
- ¹⁵M. Massetti, F. Jiao, A. J. Ferguson, D. Zhao, K. Wijeratne, A. Würger, J. L. Blackburn, X. Crispin, and S. Fabiano, "Unconventional thermoelectric materials for energy harvesting and sensing applications," *Chemical Reviews* **121**, 12465-12547 (2021).
- ¹⁶J.-C. Chiang, and A. G. MacDiarmid, "'Polyaniline': Protonic acid doping of the emeraldine form to the metallic regime," *Synth. Met.* **13**, 193-205 (1986).
- ¹⁷E. M. Thomas, E. C. Davidson, R. Katsumata, R. A. Segalman, and M. L. Chabiny, "Branched side chains govern counterion position and doping mechanism in conjugated polythiophenes," *ACS Macro Lett.* **7**, 1492-1497 (2018).

- ¹⁸B. D. Naab, S. Guo, S. Olthof, E. G. B. Evans, P. Wei, G. L. Millhauser, A. Kahn, S. Barlow, S. R. Marder, and Z. Bao, "Mechanistic study on the solution-phase n-doping of 1,3-Dimethyl-2-aryl-2,3-dihydro-1H-benzimidazole derivatives," *J. Am. Chem. Soc.* **135**, 15018-15025 (2013).
- ¹⁹S. Jhulki, H.-I. Un, Y.-F. Ding, C. Risko, S. K. Mohapatra, J. Pei, S. Barlow, and S. R. Marder, "Reactivity of an air-stable dihydrobenzimidazole n-dopant with organic semiconductor molecules," *Chem* **7**, 1050-1065 (2021).
- ²⁰R. A. Schlitz, F. G. Brunetti, A. M. Glauddell, P. L. Miller, M. A. Brady, C. J. Takacs, C. J. Hawker, and M. L. Chabiny, "Solubility-limited extrinsic n-type doping of a high electron mobility polymer for thermoelectric applications," *Adv. Mater.* **26**, 2825-2830 (2014).
- ²¹S. Riera-Galindo, A. Orbelli Biroli, A. Forni, Y. Puttisong, F. Tessore, M. Pizzotti, E. Pavlopoulou, E. Solano, S. Wang, G. Wang, T.-P. Ruoko, W. M. Chen, M. Kemerink, M. Berggren, G. di Carlo, and S. Fabiano, "Impact of singly occupied molecular orbital energy on the n-doping efficiency of benzimidazole derivatives," *ACS Appl. Mater. Interfaces* **11**, 37981-37990 (2019).
- ²²H. Guo, C.-Y. Yang, X. Zhang, A. Motta, K. Feng, Y. Xia, Y. Shi, Z. Wu, K. Yang, J. Chen, Q. Liao, Y. Tang, H. Sun, H. Y. Woo, S. Fabiano, A. Facchetti, and X. Guo, "Transition metal-catalysed molecular n-doping of organic semiconductors," *Nat. Mater.* **599**, 67-73 (2021).
- ²³A. I. Hofmann, R. Kroon, L. Yu, and C. Müller, "Highly stable doping of a polar polythiophene through co-processing with sulfonic acids and bistriflimide," *J. Mater. Chem. C* **6**, 6905-6910 (2018).
- ²⁴B. Yurash, D. X. Cao, V. V. Brus, D. Leifert, M. Wang, A. Dixon, M. Seifrid, A. E. Mansour, D. Lungwitz, T. Liu, P. J. Santiago, K. R. Graham, N. Koch, G. C. Bazan, and T.-Q. Nguyen, "Towards understanding the doping mechanism of organic semiconductors by Lewis acids," *Nat. Mater.* **18**, 1327-1334 (2019).
- ²⁵M. Arvind, C. E. Tait, M. Guerrini, J. Krumland, A. M. Valencia, C. Cocchi, A. E. Mansour, N. Koch, S. Barlow, S. R. Marder, J. Behrends, and D. Neher, "Quantitative analysis of doping-induced polarons and charge-transfer complexes of poly(3-hexylthiophene) in solution," *J. Phys. Chem. B* **124**, 7694-7708 (2020).
- ²⁶A. D. Scaccabarozzi, A. Basu, F. Aniés, J. Liu, O. Zapata-Arteaga, R. Warren, Y. Firdaus, M. I. Nugraha, Y. Lin, M. Campoy-Quiles, N. Koch, C. Müller, L. Tsetseris, M. Heeney, and T. D. Anthopoulos, "Doping approaches for organic semiconductors," *Chem. Rev.* **122**, 4420-4492 (2022).
- ²⁷W. Zhao, J. Ding, Y. Zou, C.-a. Di, and D. Zhu, "Chemical doping of organic semiconductors for thermoelectric applications," *Chem. Soc. Rev.* **49**, 7210-7228 (2020).
- ²⁸I. Salzmann, G. Heimel, M. Oehzelt, S. Winkler, and N. Koch, "Molecular electrical doping of organic semiconductors: fundamental mechanisms and emerging dopant design rules," *Acc. Chem. Res.* **49**, 370-378 (2016).

- ²⁹I. E. Jacobs, and A. J. Moulé, "Controlling molecular doping in organic semiconductors," *Adv. Mater.* **29**, 1703063 (2017).
- ³⁰T. Biskup, "Doping of organic semiconductors: Insights from EPR spectroscopy," *Applied Physics Letters* **119**, (2021).
- ³¹A. I. Hofmann, R. Kroon, S. Zokaei, E. Järsvall, C. Malacrida, S. Ludwigs, T. Biskup, and C. Müller, "Chemical doping of conjugated polymers with the strong oxidant magic blue," *Adv. Electron. Mater.* **6**, 2000249 (2020).
- ³²I. Sahalianov, J. Hynynen, S. Barlow, S. R. Marder, C. Müller, and I. Zozoulenko, "UV-to-IR Absorption of Molecularly p-Doped Polythiophenes with Alkyl and Oligoether Side Chains: Experiment and Interpretation Based on Density Functional Theory," *J. Phys. Chem. B* **124**, 11280-11293 (2020).
- ³³T. L. Murrey, M. A. Riley, G. Gonen, D. D. Antonio, L. Filardi, N. Shevchenko, M. Mascal, and A. J. Moule, "Anion Exchange Doping: Tuning Equilibrium to Increase Doping Efficiency in Semiconducting Polymers," *J. Phys. Chem. Lett.* **12**, 1284-1289 (2021).
- ³⁴D. T. Scholes, P. Y. Yee, J. R. Lindemuth, H. Kang, J. Onorato, R. Ghosh, C. K. Luscombe, F. C. Spano, S. H. Tolbert, and B. J. Schwartz, "The effects of crystallinity on charge transport and the structure of sequentially processed F₄TCNQ-doped conjugated polymer films," *Adv. Funct. Mater.* **27**, 1702654 (2017).
- ³⁵R. Ghosh, A. R. Chew, J. Onorato, V. Pakhnyuk, C. K. Luscombe, A. Salleo, and F. C. Spano, "Spectral signatures and spatial coherence of bound and unbound polarons in P3HT films: theory versus experiment," *J. Phys. Chem. C* **122**, 18048-18060 (2018).
- ³⁶J. Li, I. Duchemin, O. M. Roscioni, P. Friederich, M. Anderson, E. Da Como, G. Kociok-Köhn, W. Wenzel, C. Zannoni, D. Beljonne, X. Blase, and G. D'Avino, "Host dependence of the electron affinity of molecular dopants," *Mater. Horiz.* **6**, 107-114 (2019).
- ³⁷B. Nell, K. Ortstein, O. V. Boltalina, and K. Vandewal, "Influence of dopant–host energy level offset on thermoelectric properties of doped organic semiconductors," *J. Phys. Chem. C* **122**, 11730-11735 (2018).
- ³⁸A. Fediai, A. Emering, F. Symalla, and W. Wenzel, "Disorder-driven doping activation in organic semiconductors," *Phys. Chem. Chem. Phys.* **22**, 10256-10264 (2020).
- ³⁹I. E. Jacobs, C. Cendra, T. F. Harrelson, Z. I. Bedolla Valdez, R. Faller, A. Salleo, and A. J. Moulé, "Polymorphism controls the degree of charge transfer in a molecularly doped semiconducting polymer," *Mater. Horiz.* **5**, 655-660 (2018).
- ⁴⁰O. Zapata-Arteaga, B. Dörfling, A. Perevedentsev, J. Martín, J. S. Reparaz, and M. Campoy-Quiles, "Closing the stability–performance gap in organic thermoelectrics by adjusting the partial to integer charge transfer ratio," *Macromolecules* **53**, 609-620 (2020).

- ⁴¹H. Méndez, G. Heimel, A. Opitz, K. Sauer, P. Barkowski, M. Oehzelt, J. Soeda, T. Okamoto, J. Takeya, J.-B. Arlin, J.-Y. Balandier, Y. Geerts, N. Koch, and I. Salzmann, "Doping of organic semiconductors: Impact of dopant strength and electronic coupling," *Angew. Chem. Int. Ed.* **52**, 7751-7755 (2013).
- ⁴²H. Méndez, G. Heimel, S. Winkler, J. Frisch, A. Opitz, K. Sauer, B. Wegner, M. Oehzelt, C. Röthel, S. Duhm, D. Többens, N. Koch, and I. Salzmann, "Charge-transfer crystallites as molecular electrical dopants," *Nat. Commun.* **6**, 8560 (2015).
- ⁴³M. Goel, M. Siegert, G. Krauss, J. Mohanraj, A. Hochgesang, D. C. Heinrich, M. Fried, J. Pflaum, and M. Thelakkat, "HOMO–HOMO electron transfer: An elegant strategy for p-type doping of polymer semiconductors toward thermoelectric applications," *Adv. Mater.* **32**, 2003596 (2020).
- ⁴⁴G. Krauss, A. Hochgesang, J. Mohanraj, and M. Thelakkat, "Highly Efficient Doping of Conjugated Polymers Using Multielectron Acceptor Salts," *Macromol. Rapid Commun.* **42**, 2100443 (2021).
- ⁴⁵D. Kiefer, R. Kroon, A. I. Hofmann, H. Sun, X. Liu, A. Giovannitti, D. Stegerer, A. Cano, J. Hynynen, L. Yu, Y. Zhang, D. Nai, T. F. Harrelson, M. Sommer, A. J. Moulé, M. Kemerink, S. R. Marder, I. McCulloch, M. Fahlman, S. Fabiano, and C. Müller, "Double doping of conjugated polymers with monomer molecular dopants," *Nat. Mater.* **18**, 149-155 (2019).
- ⁴⁶H. T. Yi, N. Gartstein, and V. Podzorov, "Charge carrier coherence and Hall effect in organic semiconductors," *Sci. Rep.* **6**, 23650 (2016).
- ⁴⁷P. Pingel, and D. Neher, "Comprehensive picture of p-type doping of P3HT with the molecular acceptor F₄TCNQ," *Phys. Rev. B* **87**, 115209 (2013).
- ⁴⁸M. Schwarze, C. Gaul, R. Scholz, F. Bussolotti, A. Hofacker, K. S. Schellhammer, B. Nell, B. D. Naab, Z. Bao, D. Spoltore, K. Vandewal, J. Widmer, S. Kera, N. Ueno, F. Ortman, and K. Leo, "Molecular parameters responsible for thermally activated transport in doped organic semiconductors," *Nat. Mater.* **18**, 242-248 (2019).
- ⁴⁹A. Mityashin, Y. Olivier, T. Van Regemorter, C. Rolin, S. Verlaak, N. G. Martinelli, D. Beljonne, J. Cornil, J. Genoe, and P. Heremans, "Unraveling the mechanism of molecular doping in organic semiconductors," *Adv. Mater.* **24**, 1535-1539 (2012).
- ⁵⁰M. L. Tietze, J. Benduhn, P. Pahner, B. Nell, M. Schwarze, H. Kleemann, M. Krammer, K. Zojer, K. Vandewal, and K. Leo, "Elementary steps in electrical doping of organic semiconductors," *Nat. Commun.* **9**, 1182 (2018).
- ⁵¹A. Privitera, G. Londi, M. Riede, G. D'Avino, and D. Beljonne, "Molecular quadrupole moments promote ground-state charge generation in doped organic semiconductors," *Adv. Funct. Mater.* **30**, 2004600 (2020).
- ⁵²W. Kaiser, J. Popp, M. Rinderle, T. Albes, and A. Gagliardi, "Generalized kinetic monte carlo framework for organic electronics," *Algorithms* **11**, 37 (2018).

- ⁵³H. Abdalla, G. Zuo, and M. Kemerink, "Range and energetics of charge hopping in organic semiconductors," *Phys. Rev. B* **96**, 241202 (2017).
- ⁵⁴T. J. Aubry, J. C. Axtell, V. M. Basile, K. J. Winchell, J. R. Lindemuth, T. M. Porter, J.-Y. Liu, A. N. Alexandrova, C. P. Kubiak, S. H. Tolbert, A. M. Spokoyny, and B. J. Schwartz, "Dodecaborane-based dopants designed to shield anion electrostatics lead to increased carrier mobility in a doped conjugated polymer," *Adv. Mater.* **31**, 1805647 (2019).
- ⁵⁵Y. Karpov, T. Erdmann, I. Raguzin, M. Al-Hussein, M. Binner, U. Lappan, M. Stamm, K. L. Gerasimov, T. Beryozkina, V. Bakulev, D. V. Anokhin, D. A. Ivanov, F. Günther, S. Gemming, G. Seifert, B. Voit, R. Di Pietro, and A. Kiriya, "High conductivity in molecularly p-doped diketopyrrolopyrrole-based polymer: The impact of a high dopant strength and good structural order," *Adv. Mater.* **28**, 6003-6010 (2016).
- ⁵⁶Z. Liang, Y. Zhang, M. Souri, X. Luo, Alex M. Boehm, R. Li, Y. Zhang, T. Wang, D.-Y. Kim, J. Mei, S. R. Marder, and K. R. Graham, "Influence of dopant size and electron affinity on the electrical conductivity and thermoelectric properties of a series of conjugated polymers," *J. Mater. Chem. A* **6**, 16495-16505 (2018).
- ⁵⁷J. Li, G. Zhang, D. M. Holm, I. E. Jacobs, B. Yin, P. Stroeve, M. Mascal, and A. J. Moulé, "Introducing solubility control for improved organic p-type dopants," *Chem. Mater.* **27**, 5765-5774 (2015).
- ⁵⁸T. J. Aubry, K. J. Winchell, C. Z. Salamat, V. M. Basile, J. R. Lindemuth, J. M. Stauber, J. C. Axtell, R. M. Kubena, M. D. Phan, M. J. Bird, A. M. Spokoyny, S. H. Tolbert, and B. J. Schwartz, "Tunable dopants with intrinsic counterion separation reveal the effects of electron affinity on dopant intercalation and free carrier production in sequentially doped conjugated polymer films," *Adv. Funct. Mater.* **30**, 2001800 (2020).
- ⁵⁹I. E. Jacobs, Y. Lin, Y. Huang, X. Ren, D. Simatos, C. Chen, D. Tjhe, M. Statz, L. Lai, P. A. Finn, W. G. Neal, G. D'Avino, V. Lemaire, S. Fratini, D. Beljonne, J. Strzalka, C. B. Nielsen, S. Barlow, S. R. Marder, I. McCulloch, and H. Sirringhaus, "High-efficiency ion-exchange doping of conducting polymers," *Adv. Mater.*, 2102988 (2021).
- ⁶⁰T. Z. Ma, B. X. Dong, J. W. Onorato, J. Niklas, O. Poluektov, C. K. Luscombe, and S. N. Patel, "Correlating conductivity and Seebeck coefficient to doping within crystalline and amorphous domains in poly(3-(methoxyethoxyethoxy)thiophene)," *J. Polym. Sci.* **59**, 2797-2808 (2021).
- ⁶¹M. L. Tietze, P. Pöhner, K. Schmidt, K. Leo, and B. Lüssem, "Doped organic semiconductors: Trap-filling, impurity saturation, and reserve regimes," *Adv. Funct. Mater.* **25**, 2701-2707 (2015).
- ⁶²V. I. Arkhipov, E. V. Emelianova, P. Heremans, and H. Bässler, "Analytic model of carrier mobility in doped disordered organic semiconductors," *Phys. Rev. B* **72**, 235202 (2005).

- ⁶³V. I. Arkhipov, P. Heremans, E. V. Emelianova, and H. Bässler, "Effect of doping on the density-of-states distribution and carrier hopping in disordered organic semiconductors," *Phys. Rev. B* **71**, 045214 (2005).
- ⁶⁴G. Zuo, H. Abdalla, and M. Kemerink, "Conjugated polymer blends for organic thermoelectrics," *Adv. Electron. Mater.* **5**, 1800821 (2019).
- ⁶⁵Z. Liang, H. H. Choi, X. Luo, T. Liu, A. Abtahi, U. S. Ramasamy, J. A. Hitron, K. N. Baustert, J. L. Hempel, A. M. Boehm, A. Ansary, D. R. Strachan, J. Mei, C. Risko, V. Podzorov, and K. R. Graham, "n-type charge transport in heavily p-doped polymers," *Nat. Mater.* **20**, 518-524 (2021).
- ⁶⁶K. Xu, T. P. Ruoko, M. Shokrani, D. Scheunemann, H. Abdalla, H. D. Sun, C. Y. Yang, Y. Puttisong, N. B. Kolhe, J. S. M. Figueroa, J. O. Pedersen, T. Ederth, W. M. Chen, M. Berggren, S. A. Jenekhe, D. Fazzi, M. Kemerink, and S. Fabiano, "On the Origin of Seebeck Coefficient Inversion in Highly Doped Conducting Polymers," *Adv. Funct. Mater.*, 2112276 (2022).
- ⁶⁷D. Derewjanko, D. Scheunemann, E. Järsvall, A. I. Hofmann, C. Müller, and M. Kemerink, "Delocalization Enhances Conductivity at High Doping Concentrations," *Adv. Funct. Mater.*, 2112262 (2022).
- ⁶⁸M. Lögdlund, R. Lazzaroni, S. Stafström, W. R. Salaneck, and J. L. Brédas, "Direct observation of charge-induced π -electronic structural changes in a conjugated polymer," *Phys. Rev. Lett.* **63**, 1841-1844 (1989).
- ⁶⁹C. Gaul, S. Hutsch, M. Schwarze, K. S. Schellhammer, F. Bussolotti, S. Kera, G. Cuniberti, K. Leo, and F. Ortman, "Insight into doping efficiency of organic semiconductors from the analysis of the density of states in n-doped C_{60} and ZnPc," *Nat. Mater.* **17**, 439-444 (2018).
- ⁷⁰X. Lin, G. E. Purdum, Y. Zhang, S. Barlow, S. R. Marder, Y.-L. Loo, and A. Kahn, "Impact of a low concentration of dopants on the distribution of gap states in a molecular semiconductor," *Chem. Mater.* **28**, 2677-2684 (2016).
- ⁷¹A. Fediai, F. Symalla, P. Friederich, and W. Wenzel, "Disorder compensation controls doping efficiency in organic semiconductors," *Nat. Commun.* **10**, 4547 (2019).
- ⁷²P. Boufflet, G. Bovo, L. Occhi, H.-K. Yuan, Z. Fei, Y. Han, T. D. Anthopoulos, P. N. Stavrinou, and M. Heeney, "The influence of backbone fluorination on the dielectric constant of conjugated polythiophenes," *Adv. Electron. Mater.* **4**, 1700375 (2018).
- ⁷³B. Xu, X. Yi, T.-Y. Huang, Z. Zheng, J. Zhang, A. Salehi, V. Coropceanu, C. H. Y. Ho, S. R. Marder, M. F. Toney, J.-L. Brédas, F. So, and J. R. Reynolds, "Donor conjugated polymers with polar side chain groups: The role of dielectric constant and energetic disorder on photovoltaic performance," *Adv. Funct. Mater.* **28**, 1803418 (2018).

- ⁷⁴P. Yang, M. Yuan, D. F. Zeigler, S. E. Watkins, J. A. Lee, and C. K. Luscombe, "Influence of fluorine substituents on the film dielectric constant and open-circuit voltage in organic photovoltaics," *J. Mater. Chem. C* **2**, 3278-3284 (2014).
- ⁷⁵Y. Lu, Z. Xiao, Y. Yuan, H. Wu, Z. An, Y. Hou, C. Gao, and J. Huang, "Fluorine substituted thiophene–quinoxaline copolymer to reduce the HOMO level and increase the dielectric constant for high open-circuit voltage organic solar cells," *J. Mater. Chem. C* **1**, 630-637 (2013).
- ⁷⁶C. Wang, Z. Zhang, S. Pejić, R. Li, M. Fukuto, L. Zhu, and G. Sauvé, "High dielectric constant semiconducting poly(3-alkylthiophene)s from side chain modification with polar sulfinyl and sulfonyl groups," *Macromolecules* **51**, 9368-9381 (2018).
- ⁷⁷N. Cho, C. W. Schlenker, K. M. Kesting, P. Koelsch, H.-L. Yip, D. S. Ginger, and A. K.-Y. Jen, "High-dielectric constant side-chain polymers show reduced non-geminate recombination in heterojunction solar cells," *Adv. Energy Mater.* **4**, 1301857 (2014).
- ⁷⁸Y. Sun, S.-C. Chien, H.-L. Yip, K.-S. Chen, Y. Zhang, J. A. Davies, F.-C. Chen, B. Lin, and A. K. Y. Jen, "Improved thin film morphology and bulk-heterojunction solar cell performance through systematic tuning of the surface energy of conjugated polymers," *J. Mater. Chem.* **22**, 5587-5595 (2012).
- ⁷⁹J. Brebels, J. V. Manca, L. Lutsen, D. Vanderzande, and W. Maes, "High dielectric constant conjugated materials for organic photovoltaics," *J. Mater. Chem. A* **5**, 24037-24050 (2017).
- ⁸⁰X. Chen, Z. Zhang, Z. Ding, J. Liu, and L. Wang, "Diketopyrrolopyrrole-based conjugated polymers bearing branched oligo(ethylene glycol) side chains for photovoltaic devices," *Angew. Chem. Int. Ed.* **55**, 10376-10380 (2016).
- ⁸¹S. Torabi, F. Jahani, I. Van Severen, C. Kanimozhi, S. Patil, R. W. A. Havenith, R. C. Chiechi, L. Lutsen, D. J. M. Vanderzande, T. J. Cleij, J. C. Hummelen, and L. J. A. Koster, "Strategy for enhancing the dielectric constant of organic semiconductors without sacrificing charge carrier mobility and solubility," *Adv. Funct. Mater.* **25**, 150-157 (2015).
- ⁸²M. Lenes, F. B. Kooistra, J. C. Hummelen, I. V. Severen, L. Lutsen, D. Vanderzande, T. J. Cleij, and P. W. M. Blom, "Charge dissociation in polymer:fullerene bulk heterojunction solar cells with enhanced permittivity," *J. Appl. Phys.* **104**, 114517 (2008).
- ⁸³M. Bresselge, I. Van Severen, L. Lutsen, P. Adriaensens, J. Manca, D. Vanderzande, and T. Cleij, "Comparison of the electrical characteristics of four 2,5-substituted poly(p-phenylene vinylene) derivatives with different side chains," *Thin Solid Films* **511-512**, 328-332 (2006).
- ⁸⁴Note that p(g₄2T-T) has a lower side-chain grafting density and $IE_{osc} = 4.7$ eV compared to regioregular P3HT with $IE_{osc} = 5.1$ eV due to the electron-donating effect of the oxygen adjacent to some of the thiophene rings of p(g₄2T-T); $IE_{osc} = 5.1$ eV + e × oxidation potential measured vs. ferrocene/ferrocenium, Fc/Fc⁺.

- ⁸⁵R. Kroon, D. Kiefer, D. Stegerer, L. Yu, M. Sommer, and C. Müller, "Polar side chains enhance processability, electrical conductivity, and thermal stability of a molecularly p-doped polythiophene," *Adv. Mater.* **29**, 1700930 (2017).
- ⁸⁶I. E. Jacobs, E. W. Aasen, J. L. Oliveira, T. N. Fonseca, J. D. Roehling, J. Li, G. Zhang, M. P. Augustine, M. Mascal, and A. J. Moulé, "Comparison of solution-mixed and sequentially processed P3HT:F₄TCNQ films: effect of doping-induced aggregation on film morphology," *J. Mater. Chem. C* **4**, 3454-3466 (2016).
- ⁸⁷J. Hynynen, D. Kiefer, and C. Müller, "Influence of crystallinity on the thermoelectric power factor of P3HT vapour-doped with F₄TCNQ," *RSC Adv.* **8**, 1593-1599 (2018).
- ⁸⁸J. Hynynen, D. Kiefer, L. Yu, R. Kroon, R. Munir, A. Amassian, M. Kemerink, and C. Müller, "Enhanced electrical conductivity of molecularly p-doped poly(3-hexylthiophene) through understanding the correlation with solid-state order," *Macromolecules* **50**, 8140-8148 (2017).
- ⁸⁹A. Hamidi-Sakr, L. Biniak, J.-L. Bantignies, D. Maurin, L. Herrmann, N. Leclerc, P. Lévêque, V. Vijayakumar, N. Zimmermann, and M. Brinkmann, "A versatile method to fabricate highly in-plane aligned conducting polymer films with anisotropic charge transport and thermoelectric properties: The key role of alkyl side chain layers on the doping mechanism," *Adv. Funct. Mater.* **27**, 1700173 (2017).
- ⁹⁰E. Lim, K. A. Peterson, G. M. Su, and M. L. Chabinyk, "Thermoelectric properties of poly(3-hexylthiophene) (P3HT) doped with 2,3,5,6-tetrafluoro-7,7,8,8-tetracyanoquinodimethane (F₄TCNQ) by vapor-phase infiltration," *Chem. Mater.* **30**, 998-1010 (2018).
- ⁹¹K. Xu, H. Sun, T.-P. Ruoko, G. Wang, R. Kroon, N. B. Kolhe, Y. Puttisong, X. Liu, D. Fazzi, K. Shibata, C.-Y. Yang, N. Sun, G. Persson, A. B. Yankovich, E. Olsson, H. Yoshida, W. M. Chen, M. Fahlman, M. Kemerink, S. A. Jenekhe, C. Müller, M. Berggren, and S. Fabiano, "Ground-state electron transfer in all-polymer donor-acceptor heterojunctions," *Nat. Mater.* **19**, 738-744 (2020).
- ⁹²C. Wang, D. T. Duong, K. Vandewal, J. Rivnay, and A. Salleo, "Optical measurement of doping efficiency in poly(3-hexylthiophene) solutions and thin films," *Phys. Rev. B* **91**, 085205 (2015).
- ⁹³T. F. Harrelson, Y. Q. Cheng, J. Li, I. E. Jacobs, A. J. Ramirez-Cuesta, R. Faller, and A. J. Moulé, "Identifying atomic scale structure in undoped/doped semicrystalline P3HT using inelastic neutron scattering," *Macromolecules* **50**, 2424-2435 (2017).
- ⁹⁴D. T. Scholes, S. A. Hawks, P. Y. Yee, H. Wu, J. R. Lindemuth, S. H. Tolbert, and B. J. Schwartz, "Overcoming film quality issues for conjugated polymers doped with F₄TCNQ by solution sequential processing: Hall Effect, structural, and optical measurements," *J. Phys. Chem. Lett.* **6**, 4786-4793 (2015).

- ⁹⁵L. Müller, D. Nanova, T. Glaser, S. Beck, A. Pucci, A. K. Kast, R. R. Schröder, E. Mankel, P. Pingel, D. Neher, W. Kowalsky, and R. Lovrincic, "Charge-transfer–solvent interaction predefines doping efficiency in p-doped P3HT films," *Chem. Mater.* **28**, 4432-4439 (2016).
- ⁹⁶D. Scheunemann, and M. Kemerink, in *Organic flexible electronics*, (Eds: P. Cosseddu, M. Caironi), Woodhead Publishing, 2021, 165-197.
- ⁹⁷M. Comin, S. Fratini, X. Blase, and G. D'Avino, "Doping-Induced Dielectric Catastrophe Prompts Free-Carrier Release in Organic Semiconductors," *Adv. Mater.* **34**, 2105376 (2022).
- ⁹⁸M. Koopmans, M. A. T. Leiviskä, J. Liu, J. Dong, L. Qiu, J. C. Hummelen, G. Portale, M. C. Heiber, and L. J. A. Koster, "Electrical conductivity of doped organic semiconductors limited by carrier–carrier interactions," *ACS Appl. Mater. Interfaces* **12**, 56222-56230 (2020).
- ⁹⁹E. M. Thomas, K. A. Peterson, A. H. Balzer, D. Rawlings, N. Stingelin, R. A. Segalman, and M. L. Chabiny, "Effects of Counter-Ion Size on Delocalization of Carriers and Stability of Doped Semiconducting Polymers," *Adv. Electron. Mater.* **6**, 2000595 (2020).
- ¹⁰⁰I. E. Jacobs, G. D'Avino, V. Lemaury, Y. Lin, Y. Huang, C. Chen, T. F. Harrelson, W. Wood, L. J. Spalek, T. Mustafa, C. A. O'Keefe, X. Ren, D. Simatos, D. Tjhe, M. Statz, J. W. Strzalka, J.-K. Lee, I. McCulloch, S. Fratini, D. Beljonne, and H. Sirringhaus, "Structural and Dynamic Disorder, Not Ionic Trapping, Controls Charge Transport in Highly Doped Conducting Polymers," *J. Am. Chem. Soc.* **144**, 3005-3019 (2022).
- ¹⁰¹D. Kim, and I. Zozoulenko, "Why is pristine PEDOT oxidized to 33%? A density functional theory study of oxidative polymerization mechanism," *J. Phys. Chem. B* **123**, 5160-5167 (2019).
- ¹⁰²V. Untilova, J. Hynynen, A. I. Hofmann, D. Scheunemann, Y. Zhang, S. Barlow, M. Kemerink, S. R. Marder, L. Biniek, C. Müller, and M. Brinkmann, "High thermoelectric power factor of poly(3-hexylthiophene) through in-plane alignment and doping with a molybdenum dithiolene complex," *Macromolecules* **53**, 6314-6321 (2020).
- ¹⁰³D. T. Duong, C. Wang, E. Antono, M. F. Toney, and A. Salleo, "The chemical and structural origin of efficient p-type doping in P3HT," *Org. Electron.* **14**, 1330-1336 (2013).
- ¹⁰⁴J. E. Cochran, M. J. N. Junk, A. M. Glauddell, P. L. Miller, J. S. Cowart, M. F. Toney, C. J. Hawker, B. F. Chmelka, and M. L. Chabiny, "Molecular interactions and ordering in electrically doped polymers: Blends of PBTTT and F₄TCNQ," *Macromolecules* **47**, 6836-6846 (2014).
- ¹⁰⁵P. Y. Yee, D. T. Scholes, B. J. Schwartz, and S. H. Tolbert, "Dopant-induced ordering of amorphous regions in regiorandom P3HT," *J. Phys. Chem. Lett.* **10**, 4929-4934 (2019).
- ¹⁰⁶W. Liu, L. Müller, S. Ma, S. Barlow, S. R. Marder, W. Kowalsky, A. Köhn, and R. Lovrincic, "Origin of the π – π spacing change upon doping of semiconducting polymers," *J. Phys. Chem. C* **122**, 27983-27990 (2018).

- ¹⁰⁷J. Li, C. Koshnick, S. O. Diallo, S. Ackling, D. M. Huang, I. E. Jacobs, T. F. Harrelson, K. Hong, G. Zhang, J. Beckett, M. Mascal, and A. J. Moulé, “Quantitative measurements of the temperature-dependent microscopic and macroscopic dynamics of a molecular dopant in a conjugated polymer,” *Macromolecules* **50**, 5476-5489 (2017).
- ¹⁰⁸I. E. Jacobs, E. W. Aasen, D. Nowak, J. Li, W. Morrison, J. D. Roehling, M. P. Augustine, and A. J. Moulé, “Direct-write optical patterning of P3HT films beyond the diffraction limit,” *Adv. Mater.* **29**, 1603221 (2017).
- ¹⁰⁹V. Vijayakumar, P. Durand, H. Zeng, V. Untilova, L. Herrmann, P. Algayer, N. Leclerc, and M. Brinkmann, “Influence of dopant size and doping method on the structure and thermoelectric properties of PBTTT films doped with F₆TCNNQ and F₄TCNQ,” *J. Mater. Chem. C* **8**, 16470-16482 (2020).
- ¹¹⁰C. J. Boyle, M. Upadhyaya, P. Wang, L. A. Renna, M. Lu-Díaz, S. Pyo Jeong, N. Hight-Huf, L. Korugic-Karasz, M. D. Barnes, Z. Aksamija, and D. Venkataraman, “Tuning charge transport dynamics via clustering of doping in organic semiconductor thin films,” *Nat. Commun.* **10**, 2827 (2019).
- ¹¹¹J. Liu, L. Qiu, R. Alessandri, X. Qiu, G. Portale, J. Dong, W. Talsma, G. Ye, A. A. Sengrian, P. C. T. Souza, M. A. Loi, R. C. Chiechi, S. J. Marrink, J. C. Hummelen, and L. J. A. Koster, “Enhancing molecular n-type doping of donor–acceptor copolymers by tailoring side chains,” *Adv. Mater.* **30**, 1704630 (2018).
- ¹¹²J. Liu, L. Qiu, G. Portale, M. Koopmans, G. ten Brink, J. C. Hummelen, and L. J. A. Koster, “N-Type organic thermoelectrics: Improved power factor by tailoring host–dopant miscibility,” *Adv. Mater.* **29**, 1701641 (2017).
- ¹¹³D. Kiefer, A. Giovannitti, H. Sun, T. Biskup, A. Hofmann, M. Koopmans, C. Cendra, S. Weber, L. J. Anton Koster, E. Olsson, J. Rivnay, S. Fabiano, I. McCulloch, and C. Müller, “Enhanced n-doping efficiency of a naphthalenediimide-based copolymer through polar side chains for organic thermoelectrics,” *ACS Energy Lett.* **3**, 278-285 (2018).
- ¹¹⁴B. X. Dong, C. Nowak, J. W. Onorato, T. Ma, J. Niklas, O. G. Poluektov, G. Grocke, M. F. DiTusa, F. A. Escobedo, C. K. Luscombe, P. F. Nealey, and S. N. Patel, “Complex relationship between side-chain polarity, conductivity, and thermal stability in molecularly doped conjugated polymers,” *Chem. Mater.* **33**, 741-753 (2021).
- ¹¹⁵S. Kohno, Y. Yamashita, N. Kasuya, T. Mikie, I. Osaka, K. Takimiya, J. Takeya, and S. Watanabe, “Controlled steric selectivity in molecular doping towards closest-packed supramolecular conductors,” *Commun. Mater.* **1**, 79 (2020).

- ¹¹⁶H. Li, M. E. DeCoster, C. Ming, M. Wang, Y. Chen, P. E. Hopkins, L. Chen, and H. E. Katz, "Enhanced molecular doping for high conductivity in polymers with volume freed for dopants," *Macromolecules* **52**, 9804-9812 (2019).
- ¹¹⁷M. R. Andersson, O. Thomas, W. Mammo, M. Svensson, M. Theander, and O. Inganäs, "Substituted polythiophenes designed for optoelectronic devices and conductors," *J. Mater. Chem.* **9**, 1933-1940 (1999).
- ¹¹⁸V. Vijayakumar, E. Zaborova, L. Biniek, H. Zeng, L. Herrmann, A. Carvalho, O. Boyron, N. Leclerc, and M. Brinkmann, "Effect of alkyl side chain length on doping kinetics, thermopower, and charge transport properties in highly oriented F₄TCNQ-doped PBTBT films," *ACS Appl. Mater. Interfaces* **11**, 4942-4953 (2019).
- ¹¹⁹J. Liu, G. Ye, H. G. O. Potgieser, M. Koopmans, S. Sami, M. I. Nugraha, D. R. Villalva, H. Sun, J. Dong, X. Yang, X. Qiu, C. Yao, G. Portale, S. Fabiano, T. D. Anthopoulos, D. Baran, R. W. A. Havenith, R. C. Chiechi, and L. J. A. Koster, "Amphipathic side chain of a conjugated polymer optimizes dopant location toward efficient n-type organic thermoelectrics," *Adv. Mater.* **33**, 2006694 (2021).
- ¹²⁰D. Di Nuzzo, C. Fontanesi, R. Jones, S. Allard, I. Dumsch, U. Scherf, E. von Hauff, S. Schumacher, and E. Da Como, "How intermolecular geometrical disorder affects the molecular doping of donor-acceptor copolymers," *Nat. Commun.* **6**, 6460 (2015).
- ¹²¹E. Lim, A. M. Glauddell, R. Miller, and M. L. Chabiny, "The role of ordering on the thermoelectric properties of blends of regioregular and regiorandom poly(3-hexylthiophene)," *Adv. Electron. Mater.* **5**, 1800915 (2019).
- ¹²²A. R. Chew, R. Ghosh, Z. Shang, F. C. Spano, and A. Salleo, "Sequential doping reveals the importance of amorphous chain rigidity in charge transport of semi-crystalline polymers," *J. Phys. Chem. Lett.* **8**, 4974-4980 (2017).
- ¹²³M. T. Fontana, D. A. Stanfield, D. T. Scholes, K. J. Winchell, S. H. Tolbert, and B. J. Schwartz, "Evaporation vs solution sequential doping of conjugated polymers: F₄TCNQ doping of micrometer-thick P3HT films for thermoelectrics," *J. Phys. Chem. C* **123**, 22711-22724 (2019).
- ¹²⁴L. Yu, D. Scheunemann, A. Lund, D. Kiefer, and C. Müller, "Sequential doping of solid chunks of a conjugated polymer for body-heat-powered thermoelectric modules," *Appl. Phys. Lett.* **119**, 181902 (2021).
- ¹²⁵J. Hynynen, E. Järsvall, R. Kroon, Y. Zhang, S. Barlow, S. R. Marder, M. Kemerink, A. Lund, and C. Müller, "Enhanced thermoelectric power factor of tensile drawn poly(3-hexylthiophene)," *ACS Macro Lett.* **8**, 70-76 (2019).

- ¹²⁶S. N. Patel, A. M. Glauddell, K. A. Peterson, E. M. Thomas, K. A. O'Hara, E. Lim, and M. L. Chabinyk, "Morphology controls the thermoelectric power factor of a doped semiconducting polymer," *Sci. Adv.* **3**, e1700434 (2017).
- ¹²⁷R. Kroon, J. D. Ryan, D. Kiefer, L. Yu, J. Hynynen, E. Olsson, and C. Müller, "Bulk doping of millimeter-thick conjugated polymer foams for plastic thermoelectrics," *Adv. Funct. Mater.* **27**, 1704183 (2017).
- ¹²⁸C. Müller, C. P. Radano, P. Smith, and N. Stingelin-Stutzmann, "Crystalline–crystalline poly(3-hexylthiophene)–polyethylene diblock copolymers: Solidification from the melt," *Polymer* **49**, 3973–3978 (2008).
- ¹²⁹D. Beretta, A. Perego, G. Lanzani, and M. Caironi, "Organic flexible thermoelectric generators: from modeling, a roadmap towards applications," *Sustain. Energy & Fuels* **1**, 174–190 (2017).
- ¹³⁰A. Lund, Y. Tian, S. Darabi, and C. Müller, "A polymer-based textile thermoelectric generator for wearable energy harvesting," *J. Power Sources* **480**, 228836 (2020).
- ¹³¹J. Li, C. W. Rochester, I. E. Jacobs, S. Friedrich, P. Stroeve, M. Riede, and A. J. Moulé, "Measurement of small molecular dopant F₄TCNQ and C₆₀F₃₆ diffusion in organic bilayer architectures," *ACS Appl. Mater. Interfaces* **7**, 28420–28428 (2015).
- ¹³²J. Li, C. W. Rochester, I. E. Jacobs, E. W. Aasen, S. Friedrich, P. Stroeve, and A. J. Moule, "The effect of thermal annealing on dopant site choice in conjugated polymers," *Org. Electron.* **33**, 23–31 (2016).
- ¹³³K. E. Watts, B. Neelamraju, M. Moser, I. McCulloch, E. L. Ratcliff, and J. E. Pemberton, "Thermally induced formation of HF₄TCNQ⁻ in F₄TCNQ-doped regioregular P3HT," *J. Phys. Chem. Lett.* **11**, 6586–6592 (2020).
- ¹³⁴K. E. Watts, B. Neelamraju, E. L. Ratcliff, and J. E. Pemberton, "Stability of charge transfer states in F₄TCNQ-doped P3HT," *Chem. Mater.* **31**, 6986–6994 (2019).
- ¹³⁵D. Nava, Y. Shin, M. Massetti, X. Jiao, T. Biskup, M. S. Jagadeesh, A. Calloni, L. Duò, G. Lanzani, C. R. McNeill, M. Sommer, and M. Caironi, "Drastic improvement of air stability in an n-type doped naphthalene-diimide polymer by thionation," *ACS Appl. Energy Mater.* **1**, 4626–4634 (2018).
- ¹³⁶S. Wang, T.-P. Ruoko, G. Wang, S. Riera-Galindo, S. Hultmark, Y. Puttison, F. Moro, H. Yan, W. M. Chen, M. Berggren, C. Müller, and S. Fabiano, "Sequential doping of ladder-type conjugated polymers for thermally stable n-type organic conductors," *ACS Appl. Mater. Interfaces* **12**, 53003–53011 (2020).
- ¹³⁷C.-Y. Yang, Y.-F. Ding, D. Huang, J. Wang, Z.-F. Yao, C.-X. Huang, Y. Lu, H.-I. Un, F.-D. Zhuang, J.-H. Dou, C.-a. Di, D. Zhu, J.-Y. Wang, T. Lei, and J. Pei, "A thermally activated and highly miscible dopant for n-type organic thermoelectrics," *Nat. Commun.* **11**, 3292 (2020).
- ¹³⁸C.-Y. Yang, M.-A. Stoeckel, T.-P. Ruoko, H.-Y. Wu, X. Liu, N. B. Kolhe, Z. Wu, Y. Puttison, C. Musumeci, M. Massetti, H. Sun, K. Xu, D. Tu, W. M. Chen, H. Y. Woo, M. Fahlman, S. A. Jenekhe, M.

- Berggren, and S. Fabiano, "A high-conductivity n-type polymeric ink for printed electronics," *Nat. Commun.* **12**, 2354 (2021).
- ¹³⁹Y. Lu, Z. D. Yu, H. I. Un, Z. F. Yao, H. Y. You, W. Jin, L. Li, Z. Y. Wang, B. W. Dong, S. Barlow, E. Longhi, C. A. Di, D. Zhu, J. Y. Wang, C. Silva, S. R. Marder, and J. Pei, "Persistent conjugated backbone and disordered lamellar packing impart polymers with efficient n-doping and high conductivities," *Adv. Mater.* **33**, 2005946 (2021).
- ¹⁴⁰J. Liu, G. Ye, B. V. Zee, J. Dong, X. Qiu, Y. Liu, G. Portale, R. C. Chiechi, and L. J. A. Koster, "N-Type organic thermoelectrics of donor-acceptor copolymers: Improved power factor by molecular tailoring of the density of states," *Adv. Mater.* **30**, 1804290 (2018).
- ¹⁴¹E. M. Thomas, B. C. Popere, H. Fang, M. L. Chabiny, and R. A. Segalman, "Role of disorder induced by doping on the thermoelectric properties of semiconducting polymers," *Chem. Mater.* **30**, 2965-2972 (2018).
- ¹⁴²G. Zuo, X. Liu, M. Fahlman, and M. Kemerink, "High seebeck coefficient in mixtures of conjugated polymers," *Adv. Funct. Mater.* **28**, 1703280 (2018).
- ¹⁴³A. Abtahi, S. Johnson, S. M. Park, X. Luo, Z. Liang, J. Mei, and K. R. Graham, "Designing π -conjugated polymer blends with improved thermoelectric power factors," *J. Mater. Chem. A* **7**, 19774-19785 (2019).
- ¹⁴⁴R. Sarabia-Riquelme, M. Shahi, J. W. Brill, and M. C. Weisenberger, "Effect of drawing on the electrical, thermoelectrical, and mechanical properties of wet-spun PEDOT:PSS fibers," *ACS Appl. Polym. Mater.* **1**, 2157-2167 (2019).
- ¹⁴⁵Q. Wei, M. Mukaida, K. Kirihaara, and T. Ishida, "Experimental studies on the anisotropic thermoelectric properties of conducting polymer films," *ACS Macro Lett.* **3**, 948-952 (2014).
- ¹⁴⁶Y. Kim, A. Lund, H. Noh, A. I. Hofmann, M. Craighero, S. Darabi, S. Zokaei, J. I. Park, M.-H. Yoon, and C. Müller, "Robust PEDOT:PSS wet-spun fibers for thermoelectric textiles," *Macromol. Mater. Eng.* **305**, 1900749 (2020).
- ¹⁴⁷D. Scheunemann, V. Vijayakumar, H. Zeng, P. Durand, N. Leclerc, M. Brinkmann, and M. Kemerink, "Rubbing and drawing: Generic ways to improve the thermoelectric power factor of organic semiconductors?," *Adv. Electron. Mater.* **6**, (2020).
- ¹⁴⁸V. Untilova, T. Biskup, L. Biniek, V. Vijayakumar, and M. Brinkmann, "Control of chain alignment and crystallization helps enhance charge conductivities and thermoelectric power factors in sequentially doped P3HT:F₄TCNQ films," *Macromolecules* **53**, 2441-2453 (2020).
- ¹⁴⁹S. Hwang, W. J. Potscavage, Y. S. Yang, I. S. Park, T. Matsushima, and C. Adachi, "Solution-processed organic thermoelectric materials exhibiting doping-concentration-dependent polarity," *Phys. Chem. Chem. Phys.* **18**, 29199-29207 (2016).

- ¹⁵⁰C. Y. Yang, W. L. Jin, J. Wang, Y. F. Ding, S. Nong, K. Shi, Y. Lu, Y. Z. Dai, F. D. Zhuang, T. Lei, C. A. Di, D. Zhu, J. Y. Wang, and J. Pei, "Enhancing the n-type conductivity and thermoelectric performance of donor-acceptor copolymers through donor engineering," *Adv. Mater.* **30**, e1802850 (2018).
- ¹⁵¹H. Zeng, M. Mohammed, V. Untilova, O. Boyron, N. Berton, P. Limelette, B. Schmaltz, and M. Brinkmann, "Fabrication of oriented n-type thermoelectric polymers by polarity switching in a DPP-based donor-acceptor copolymer doped with FeCl₃," *Adv. Electron. Mater.* **7**, (2021).
- ¹⁵²J. M. Ziman, *Principles of the theory of solids*, Cambridge University Press, Cambridge 1972.
- ¹⁵³R. Franz, and G. Wiedemann, "Ueber die Wärme-Leitungsfähigkeit der Metalle," *Annalen der Physik* **165**, 497-531 (1853).
- ¹⁵⁴J. Liu, X. Wang, D. Li, N. E. Coates, R. A. Segalman, and D. G. Cahill, "Thermal conductivity and elastic constants of PEDOT:PSS with high electrical conductivity," *Macromolecules* **48**, 585-591 (2015).
- ¹⁵⁵A. Weathers, Z. U. Khan, R. Brooke, D. Evans, M. T. Pettes, J. W. Andreasen, X. Crispin, and L. Shi, "Significant electronic thermal transport in the conducting polymer poly(3,4-ethylenedioxythiophene)," *Adv. Mater.* **27**, 2101-2106 (2015).
- ¹⁵⁶M. B. Salamon, J. W. Bray, G. DePasquali, R. A. Craven, G. Stucky, and A. Schultz, "Thermal conductivity of tetrathiafulvalene-tetracyanoquinodimethane (TTF-TCNQ) near the metal-insulator transition," *Phys. Rev. B* **11**, 619-622 (1975).
- ¹⁵⁷A. Miller, and E. Abrahams, "Impurity conduction at low concentrations," *Phys. Rev.* **120**, 745-755 (1960).
- ¹⁵⁸G. T. Craven, and A. Nitzan, "Wiedemann-Franz law for molecular hopping transport," *Nano Lett.* **20**, 989-993 (2020).
- ¹⁵⁹D. Scheunemann, and M. Kemerink, "Non-Wiedemann-Franz behavior of the thermal conductivity of organic semiconductors," *Phys. Rev. B* **101**, 075206 (2020).
- ¹⁶⁰R. Schmechel, "Hopping transport in doped organic semiconductors: A theoretical approach and its application to p-doped zinc-phthalocyanine," *J. Appl. Phys.* **93**, 4653-4660 (2003).
- ¹⁶¹S. Ihnatsenka, X. Crispin, and I. V. Zozoulenko, "Understanding hopping transport and thermoelectric properties of conducting polymers," *Phys. Rev. B* **92**, 035201 (2015).
- ¹⁶²O. Zapata-Arteaga, A. Perevedentsev, S. Marina, J. Martin, J. S. Reparaz, and M. Campoy-Quiles, "Reduction of the lattice thermal conductivity of polymer semiconductors by molecular doping," *ACS Energy Lett.* **5**, 2972-2978 (2020).
- ¹⁶³X. Wang, C. D. Liman, N. D. Treat, M. L. Chabinyk, and D. G. Cahill, "Ultralow thermal conductivity of fullerene derivatives," *Phys. Rev. B* **88**, 075310 (2013).
- ¹⁶⁴J. Liu, B. van der Zee, R. Alessandri, S. Sami, J. Dong, M. I. Nugraha, A. J. Barker, S. Rousseva, L. Qiu, X. Qiu, N. Klasen, R. C. Chiechi, D. Baran, M. Caironi, T. D. Anthopoulos, G. Portale, R. W. A. Havenith,

- S. J. Marrink, J. C. Hummelen, and L. J. A. Koster, "N-type organic thermoelectrics: demonstration of $ZT > 0.3$," *Nat. Commun.* **11**, 5694 (2020).
- ¹⁶⁵D. Beretta, A. J. Barker, I. Maqueira-Albo, A. Calloni, G. Bussetti, G. Dell'Erba, A. Luzio, L. Duò, A. Petrozza, G. Lanzani, and M. Caironi, "Thermoelectric properties of highly conductive Poly(3,4-ethylenedioxythiophene) polystyrene sulfonate printed thin films," *ACS Appl. Mater. Interfaces* **9**, 18151-18160 (2017).
- ¹⁶⁶T. Degousée, V. Untilova, V. Vijayakumar, X. Xu, Y. Sun, M. Palma, M. Brinkmann, L. Biniak, and O. Fenwick, "High thermal conductivity states and enhanced figure of merit in aligned polymer thermoelectric materials," *J. Mater. Chem. A* **9**, 16065-16075 (2021).